frontiers

Spiking and membrane properties of rat olfactory bulb dopamine neurons

Kirill S. Korshunov[1*], Laura J. Blakemore[1], Richard Bertram[1], Paul Q. Trombley[1]

[1]Florida State University, United States

Submitted to Journal:
Frontiers in Cellular Neuroscience

Specialty Section:
Cellular Neurophysiology

Article type:
Original Research Article

Manuscript ID:
512967

Received on:
18 Nov 2019

Revised on:
20 Feb 2020

Frontiers website link:
www.frontiersin.org

Conflict of interest statement

The authors declare that the research was conducted in the absence of any commercial or financial relationships that could be construed as a potential conflict of interest

Author contribution statement

KSK, LJB, RB, and PQT designed the experiments. KSK performed the experiments and collected data. KSK, LJB, RB, and PQT analyzed the data. KSK wrote the first draft of the manuscript. All authors contributed to subsequent drafts.

Keywords

Dopamine, Olfactory Bulb, Electrophysiology, Membrane properties, h-current, Na+ Current, Ramp protocol

Abstract

Word count: 349

The mammalian olfactory bulb (OB) has a vast population of dopamine (DA) neurons, whose function is to increase odor discrimination through mostly inhibitory synaptic mechanisms. However, it is not well understood whether there is more than one neuronal type of OB DA neuron, how these neurons respond to different stimuli, and the ionic mechanisms behind those responses. In this study, we used a transgenic rat line (hTH-GFP) to identify fluorescent OB DA neurons for recording via whole-cell electrophysiology. These neurons were grouped based on their localization in the glomerular layer ("Top" vs. "Bottom") with these largest and smallest neurons grouped by neuronal area ("Large" vs. "Small," in μm2). We found that some membrane properties could be distinguished based on a neuron's area, but not by its glomerular localization. All OB DA neurons produced a single action potential when receiving a sufficiently depolarizing stimulus, while some could also spike multiple times when receiving weaker stimuli, an activity that was more likely in Large than Small neurons. This single spiking activity is likely driven by the Na+ current, which showed a sensitivity to inactivation by depolarization and a relatively long time constant for the removal of inactivation. These recordings showed that Small neurons were more sensitive to inactivation of Na+ current at membrane potentials of -70 mV and -60 mV than Large neurons. The hyperpolarization-activated H-current (identified by voltage sags) was more pronounced in Small than Large DA neurons across hyperpolarized membrane potentials. Lastly, to mimic a more physiological stimulus, these neurons received ramp stimuli of various durations and current amplitudes. When stimulated with weaker/shallow ramps, the neurons needed less current to begin and end firing and they produced more action potentials at a slower frequency. These spiking properties were further analyzed between the four groups of neurons, and these analyses support the difference in spiking induced with current step stimuli. Thus, there may be more than one type of OB DA neuron, and these neurons' activities may support a possible role of being high-pass filters in the OB by allowing the transmission of stronger odor signals while inhibiting weaker ones.

Contribution to the field

The mammalian olfactory bulb receives odor signals from the nasal epithelium and is the first site of odor processing. The olfactory bulb uses a variety of neurons, including dopamine neurons, to modify these signals. Dopamine neurons are known to inhibit other olfactory bulb neurons, causing inhibition of certain odors while other odors are processed by higher brain regions. In the current literature, however, little is known about how these neurons specifically respond to different odor signals, and more information is needed regarding the different types of dopamine neurons present in the olfactory bulb. We use a transgenic rat line, which produces fluorescent dopamine neurons, to record their activity in response to artificial stimuli that mimic natural odor stimuli and to differentiate between different dopamine neuron types based on their localization in different parts of an olfactory bulb layer and their size. We found that these neurons appear to be more responsive to weaker than stronger odors, and that they may have different properties based on their size, but not necessarily their location. These results advance understanding of how olfactory bulb dopamine neurons may be classified, how they may process different odor signals, and how this may impact overall odor processing.

Funding statement

This research was supported by the FSU Chemical Senses Training (CTP) Grant Award T32 DC000044 from the National Institutes of Health (NIH/NIDCD) to K. Korshunov and by the National Science Foundation (NSF) grant DMS 1853342 to R. Bertram.

Ethics statements

Studies involving animal subjects
Generated Statement: The animal study was reviewed and approved by Florida State University Animal Care and Use Committee.

Studies involving human subjects
Generated Statement: No human studies are presented in this manuscript.

Inclusion of identifiable human data
Generated Statement: No potentially identifiable human images or data is presented in this study.

Data availability statement

Generated Statement: The datasets generated for this study are available on request to the corresponding author.

Spiking and membrane properties of rat olfactory bulb dopamine neurons

Kirill S. Korshunov[1, 2], Laura J. Blakemore[1, 2], Richard Bertram[1, 3], Paul Q. Trombley[1, 2].

[1]Program in Neuroscience, Florida State University, Tallahassee, FL, USA.

[2]Department of Biological Science, Florida State University, Tallahassee, FL, USA.

[3]Department of Mathematics, Florida State University, Tallahassee, FL, USA.

Corresponding author:

Kirill S. Korshunov

Florida State University,

Department of Biological Science,

3011 King Life Science Building,

319 Stadium Drive,

Tallahassee, FL 32306-4295

USA

Telephone: (850) 644-1614

Email: kkorshunov@neuro.fsu.edu

Word count: 11,127 words

Figure count: 7 figures

Abbreviations

aCSF, artificial cerebrospinal fluid; AIS, axon initial segment; Ca_v, voltage-gated Ca^{2+} channels; Cd, cadmium; Cs, cesium; DA, dopamine; EPSP, excitatory postsynaptic potential; ETC, external tufted cell; EPL, external plexiform layer; GABA, γ-amino butyric acid; GAD, glutamic acid decarboxylase; GCL, granule cell layer; GL, glomerular layer; HCN, hyperpolarization-activated cyclic nucleotide-gated channel; hTH-GFP, tyrosine hydroxylase green fluorescent protein; I_{Ca}^{2+}, Ca^{2+} current; I_H, H-current; I_{Na}, Na^+ current; IPI, interpulse interval; JGC, juxtaglomerular cell; M/TC, mitral/tufted cell; MCL, mitral cell layer; Na_v, voltage-gated Na^+ channels; OB, olfactory bulb; ONL, olfactory nerve layer; OSN, olfactory sensory neuron; P, postnatal day; PD, Parkinson's disease; PGC, periglomerular cell; SAC, short-axon cell; SEM, standard error of the mean; TH, tyrosine hydroxylase; V_f, final voltage; V_i, initial voltage

Abstract

The mammalian olfactory bulb (OB) has a vast population of dopamine (DA) neurons, whose function is to increase odor discrimination through mostly inhibitory synaptic mechanisms. However, it is not well understood whether there is more than one neuronal type of OB DA neuron, how these neurons respond to different stimuli, and the ionic mechanisms behind those responses. In this study, we used a transgenic rat line (hTH-GFP) to identify fluorescent OB DA neurons for recording via whole-cell electrophysiology. These neurons were grouped based on their localization in the glomerular layer ("Top" vs. "Bottom") with these largest and smallest neurons grouped by neuronal area ("Large" vs. "Small," in μm^2). We found that some membrane properties could be distinguished based on a neuron's area, but not by its glomerular localization. All OB DA neurons produced a single action potential when receiving a sufficiently depolarizing stimulus, while some could also spike multiple times when receiving weaker stimuli, an activity that was more likely in Large than Small neurons. This single spiking activity is likely driven by the Na^+ current, which showed a sensitivity to inactivation by depolarization and a relatively long time constant for the removal of inactivation. These recordings showed that Small neurons were more sensitive to inactivation of Na^+ current at membrane potentials of -70 mV and -60 mV than Large neurons. The hyperpolarization-activated H-current (identified by voltage sags) was more pronounced in Small than Large DA neurons across hyperpolarized membrane potentials. Lastly, to mimic a more physiological stimulus, these neurons received ramp stimuli of various durations and current amplitudes. When stimulated with weaker/shallow ramps, the neurons needed less current to begin and end firing and they produced more action potentials at a slower frequency. These spiking properties were further analyzed between the four groups of neurons, and these analyses support the difference in spiking induced with current step stimuli. Thus, there may be more than one type of OB DA neuron, and these neurons' activities may support a possible role of being high-pass filters in the OB by allowing the transmission of stronger odor signals while inhibiting weaker ones.

Keywords: dopamine, olfactory bulb, electrophysiology, membrane properties, H-current, Na^+ current, ramp protocols

Introduction

Olfaction is central to the perception of chemical environments and is a necessary sensory system for the survival of most animals. The olfactory bulb (OB) is the first region of the brain to receive and modify odor signals before sending them to higher brain regions. In many ways similar to the retina, the OB accomplishes its tasks by utilizing different subtypes of neurons embedded in distinct laminae. The neuronal circuitry and synaptic activities within the OB are complex. Chemical odors are first transduced by the olfactory sensory neurons (OSNs) in the olfactory epithelium. OSNs form glutamatergic axodendritic synapses (Berkowicz et al., 1994; Ennis et al., 1996) with interneurons of the glomerular layer (GL) and the main output neurons of the OB, mitral and tufted cells (M/TCs) (Bardoni et al., 1996a, 1996b; Keller et al., 1998; Kosaka et al., 1997; Pinching and Powell, 1971). The interneurons found in the GL are collectively termed juxtaglomerular cells (JGCs), which can be divided into three types: periglomerular cells (PGCs), short-axon cells (SACs), and external tufted cells (ETCs) (Golgi, 1875; Nagayama et al., 2014; Pinching and Powell, 1971; Shepherd, 1972; Shepherd et al., 2011). As the odor signal is being transmitted to the M/TCs, the JGCs modify the signal by the release of neurotransmitters such as glutamate, γ-amino butyric acid (GABA), and dopamine (DA).

Endogenous to the GL, DA-releasing JGCs are localized around the spherical, dense neuropil structures called glomeruli. DA is expressed in 10-16% of all JGCs; this corresponds to roughly 88,000 neurons in the GL of the OB of the mouse and roughly 100,000 neurons in the GL of the rat (McLean and Shipley, 1988; Panzanelli et al., 2007; Parrish-Aungst et al., 2007). The DA neuron population in the OB is estimated to be the largest in the entire brain (Cave and Baker, 2009). These neurons mainly make inhibitory contacts with the OSNs and the apical dendrites of M/TCs (Berkowicz and Trombley, 2000; Davila et al., 2003; Ennis et al., 2001; Hsia et al., 1999; Nickell et al., 1994; Vaaga et al., 2017). Functionally, these DA neurons are important for increasing odor resolution by simultaneously increasing odor discrimination and decreasing odor noise (Ennis et al., 2001; Tillerson et al., 2006; Wilson and Sullivan, 1995). Thus, the gating mechanisms of OB DA neurons are crucial, but it is not fully understood how these neurons respond to specific signal stimuli.

Recent studies show that OB DA neurons fall into two categories: larger neurons possessing an axon and smaller neurons that are anaxonic (Chand et al., 2015; Galliano et al.,

2018). These results support earlier reports (Halász et al., 1981; Kosaka and Kosaka, 2007, 2008, 2009; Pignatelli et al., 2005) and reviews (Kosaka and Kosaka 2011, 2016; Pignatelli & Belluzi 2017) describing two distinct sizes of OB DA neurons. What is/are the potential identities and locations of these small and large DA neurons? Based on different neuronal features, many studies often categorize OB DA neurons as being either PGCs (Kosaka et al., 1995, 1997, 1998; Kosaka and Kosaka, 2007; Parrish-Aungst et al., 2007) or SACs (Bywalez et al., 2017; Kiyokage et al., 2010; Liu et al., 2013; Cockerham et al. 2016), with SACs having a slightly larger soma size than PGCs (Nagayama et al., 2014; Pinching and Powell, 1971). A subgroup of potential DAergic PGCs were identified as the "Type-1" PGCs, which express tyrosine hydroxylase (TH; the rate-limiting enzyme present in all DA neurons) and receive excitatory input from the "ON Zone," corresponding to the area between the middle and the superficial (olfactory nerve layer [ONL]/GL) border of the glomerulus (Kosaka et al., 1995, 1997, 1998; Kosaka and Kosaka, 2007). A potential DAergic population of SACs provide the most common source of interglomerular projections in the OB (Aungst et al., 2003; Kiyokage et al., 2010), thus, may correspond to the axonic DA neurons, which are mostly found in the deeper (closer to the external plexiform layer [EPL]) portion of the GL (Galliano et al., 2018). Therefore, to distinguish between these two potential types of OB DA neurons, we used whole-cell electrophysiology to investigate differences in the membrane properties of OB DA neurons based on their laminar localization in the GL and size (neuronal area).

The response of a neuron to artificial stimuli can be indicative of both how that neuron responds to natural stimuli and the functional outcomes in the neuronal circuit. Surprisingly, there is a lack of information regarding how OB DA neurons respond to artificial stimuli. Therefore, another focus of this study was to determine the firing and gating properties of OB DA neurons in response to evoked current step stimuli. Further, the ionic currents that directly and indirectly contribute to spiking properties – Na^+ current (I_{Na}) and the nonspecific cation H-current (I_H), respectively (Iseppe et al., 2016; Pignatelli et al., 2013) – were examined in these neurons. To potentially further distinguish between types of OB DA neurons, these properties were also studied in neurons categorized according to laminar (GL) localization and neuronal area.

Lastly, the signal processing properties of OB DA neurons were investigated. These neurons are mostly inhibitory and, upon activation, release DA and the inhibitory

neurotransmitter GABA, which most OB DA neurons co-express (Baker et al., 1988; Borisovska et al., 2013; Gall et al., 1987; Kosaka et al., 1985, 1995; Liu et al., 2013, 2016; Maher and Westbrook, 2008). These inhibitory actions could increase odor discrimination through the activity of the D_2 receptor (Tillerson et al., 2006). It has been shown that higher odor concentrations increase odor discrimination (Wei et al., 2006). To investigate whether the OB DA neurons contribute to this, we used a whole-cell current-clamp recording protocol that injected ramps of current into the neurons, with variable ramp slopes. Unlike the conventional step protocols, these ramp protocols are more akin to the summation properties of natural stimuli. In combination with the conventional step stimulations, the ramp stimuli allowed us to determine how responsive OB DA neurons are to strong and weak stimuli. These responses were also differentiated between OB DA neurons based on their GL localization and neuronal area.

As many previous studies have characterized OB DA neurons in transgenic mice (Pignatelli et al., 2005, 2009, 2013; Puopolo et al., 2005), the last goal of this study was to determine these properties in the rat. Rats offer some clear advantages over mice (e.g., easier to handle, lower susceptibility to stress, larger brain size facilitates brain surgery and imaging) and are better models for the study of some human behaviors and conditions (Ellenbroek and Youn, 2016). For these experiments, we used a transgenic rat line – the TH green fluorescent protein (hTH-GFP) line (Iacovitti et al., 2014) – which expresses GFP in all TH+ (DA) neurons in the OB and other regions of the brain. The advent of this transgenic rat model has important implications to future research and facilitates the exploration of species differences (see Discussion). Whereas previous research in the rat OB characterized the biophysical properties of JGCs without determining the cell type (DA or other) (e.g., Puopolo and Belluzzi, 1998), our transgenic rat model allowed us to directly examine the electrophysiological properties of fluorescent OB DA neurons and to determine potential differences between rat and mouse OB DA neurons.

Overall, our results show that OB DA neurons may have spiking properties that differ from those of other OB neurons. These spiking properties, along with their membrane properties, I_H, and gating properties, may differ between neurons based on the neuronal area, but not necessarily the localization of these neurons in the GL. Given that OB DA neurons appear to be more responsive to weaker stimuli and are inhibitory, these results also imply that these neurons act as high-pass filters in the OB. Additionally, these spiking properties are characteristic of DA

neurons of rats, but not mice. These findings provide further insight not only to the identity of the OB DA neurons, but also to their signal processing properties that allow them to respond to different odor signals to properly process information in the rat OB.

Materials and Methods

Animals

Transgenic hTH-GFP Sprague Dawley rats (Iacovatti et al. 2014) were used for all experiments (Taconic Biosciences, USA). Rats were housed in an animal vivarium facility at Florida State University, exposed to a 12-hour light and dark cycle, and provided *ad libitum* access to food and water. All experiments were carried out in accordance with the current edition (8^{th}) of the National Institutes of Health Guide for the Care and Use of Laboratory Animals, and the Florida State University Institutional Animal Care and Use Committee approved all procedures.

Olfactory bulb dissection

Rat OB tissue slices were prepared as previously described (Blakemore et al., 2006). Rats between the ages of postnatal day (P)12 and P22 were used. A total of 83 rats were used for these experiments (approximately 2 rats for each day of recording). Animals were anesthetized with isoflurane (Henry Schein Animal Health, Dublin, OH, USA) and were decapitated. OBs were harvested in ice cold, oxygenated (95% O_2, 5% CO_2) artificial cerebrospinal fluid with sucrose (sucrose aCSF). The makeup of the sucrose aCSF solution is as follows (in mM): 83 NaCl, 2.5 KCl, 26.2 $NaHCO_3$, 1 NaH_2PO_4, 0.5 $CaCl_2$, 3.3 $MgCl_2$, 22 glucose, and 72 sucrose. OBs were glued onto a metal pedestal using cyanoacrylate and 300-µm thick horizontal slices were cut with a Vibratome (St Louis, MO, USA) in ice-cold sucrose aCSF solution. Slices were gently transferred to a holding chamber, incubated in 35° C-oxygenated aCSF solution for 30 minutes, and then stored at 20-24° C until use. The makeup of the aCSF solution is as follows (in mM): 125 NaCl, 2.5 KCl, 25 $NaHCO_3$, 1.25 NaH_2PO_4, 2 $CaCl_2$, 1 $MgCl_2$, and 25 glucose. Tissue slices were then transferred to a recording chamber for all electrophysiology experiments.

Electrophysiology

For all electrophysiology experiments, 300-µm horizontal OB slices were used for recordings in whole-cell current- and voltage-clamp modes. A Multiclamp 700B amplifier (Molecular

Devices, Axon Instruments, San Jose, CA, USA), ITC-18 digitizer (Instrutech, Longmont, CO, USA), and AxographX acquisition software (John Clements) were used for all data acquisition. Neurons were visualized with a Leica DMLFS fluorescent microscope (Meyer Instruments, Houston, TX, USA) and a Hitachi HV-D30 camera (B&H, NY, USA).

Borosilicate glass (World Precision Instruments, Sarasota, FL, USA) was pulled into electrodes with a final resistance of 4-6 MΩ. The intracellular solution for most whole-cell recordings was composed of the following (in mM): 125 $KMeSO_4$, 0.025 $CaCl_2$, 2 $MgCl_2$, 1 EGTA, 2 Na_2ATP, 0.5 NaGTP, and 10 HEPES. Neurons were constantly perfused with an oxygenated aCSF solution at a rate of 1 ml per minute. In total, we recorded from 140 neurons from OB slices. Extracellular drugs were delivered by bath perfusion. We used 25 µM $CdCl_2$ to inhibit voltage-gated calcium channels (Ca_v) for I_{Na} analyses. In addition, 5 µg/ml of propidium iodide was used to visualize the OB layers, which was incubated with post-recorded slices for 2 hours in 20-24 °C before being imaged with a Leica DMLB fluorescent microscope (Meyer Instruments, Houston, TX, USA) and an Andor camera (Andor, Oxford Instruments, Europe), with the NIS Elements AR 3.2 software (Nikon, Melville, NY, USA).

Calculating membrane properties

Membrane properties of OB DA neurons were compared based on their localization in the GL ("Top" vs. "Bottom") and neuronal areas ("Large" vs. "Small" neurons). The localization of DA neurons in the GL was distinguished visually before targeting them for whole-cell electrophysiology recordings. "Top" DA neurons were identified as the fluorescent neurons in the "upper half" (the area between the center and the ONL/GL border) of their respective glomeruli. "Bottom" DA neurons were identified as the fluorescent neurons in the "bottom half" (the area between the center and the GL/EPL border) of their respective glomeruli. We recorded from a total of 94 neurons (45 Top and 49 Bottom) categorized in this manner. (The rest of the recorded neurons were not identified by their localization or neuronal area and were thus excluded from these and subsequent calculations.)

Of the total of 140 neurons from which we recorded in slice, we determined neuronal areas ("areas") for 87 of these neurons. For the purpose of analysis, these neurons were categorized according to size and separated into thirds. As large versions of the "Small" neurons could overlap with small versions of the "Large" neurons, we eliminated the middle group of

neurons from this analysis to reduce misidentification of cells. Therefore, one-third (n = 29) of the neurons with the largest areas (3390 to 4890 μm^2) and one-third (n = 27) of the neurons with the smallest areas (1589 to 2610 μm^2) were used for calculations and comparisons of membrane properties based on neuronal area. All membrane properties were calculated from current-clamp voltage traces.

Membrane resistance was calculated by analyzing the hyperpolarizing voltage deflection in response to current injection (-10, -25, -50, or -75 pA step) using V= IR. The time constant (τ) was calculated by analyzing the amount of time it took for the neuron to hyperpolarize to 63% of its total voltage step. Capacitance was then derived using $\tau = RC$. From the capacitance, the neuronal area was calculated by $C = AC_m$. The C_m (specific capacitance) was previously determined to be 1.0 $\frac{\mu F}{cm2}$ (Gentet et al., 2000; Hodgkin and Huxley, 1952; Holohean et al., 1996), which was converted to 0.01 $\frac{pF}{\mu m2}$, the value used for these calculations. The neurons' action potential thresholds were determined through specific protocols. The first protocol injected 40, 3-ms depolarizing currents, at 1.5 second increments, with each incremental injection being 10 pA more depolarizing than the last (beginning with 10 pA and ending with 400 pA). The action potential threshold was defined as the amount of current that produced a voltage spike distinct from an Ohmic response. If the first protocol did not produce spiking in a neuron, a second protocol was used with the same specifications, except the injections were increased to increments of 20 pA (beginning with 20 pA and ending with 800 pA). Finally, voltage sag ratios were calculated by analyzing the minimum (V_i) and final (V_f) membrane voltages of a hyperpolarization step. The V_i is the value of the voltage drop before the depolarization sag, while the V_f is the voltage value at the very end of a hyperpolarizing stimulus (voltage sag ratio $= \frac{V_i - V_f}{V_i}$). All calculations were made on voltage drops produced by -25, -50, and -75 pA stimuli.

Na^+ current properties

For the recording of the I_{Na}, the intracellular recording solution consisted of the following (in mM): 125 CsCl, 2 $MgCl_2$, 1.1 EGTA, 2 ATP, 0.5 GTP, and 10 HEPES. To isolate these inward currents from the inward Ca^{2+} currents (I_{Ca}^{2+}), recordings were made in the presence of 25 µM $CdCl_2$ in the extracellular aCSF solution. All I_{Na}s were elicited by depolarizing the neuronal membrane with 200-ms, 10-mV voltage steps. I_{Na} was identified as a transient fast-activating and

inactivating inward current that would last no longer than 10 ms. The current-voltage I_{Na} curve was constructed by taking the peak current values at each depolarization step (ranging from -80 to 30 mV). To calculate the inactivation ($h\infty$) curve, the neuronal membrane received 7 50-ms pre-pulse voltage steps (ranging from -90 to -30 mV, in 10 mV increments), followed by a 100-ms 80 mV depolarizing step. The currents that resulted at the 80-mV step were used to calculate the inactivation curve. The I_{Na} with the largest amplitude, occurring when the membrane went from -90 to 80 mV, was used as a reference peak. At this point, the peak of each subsequent current (-80, -70 mV, etc.) was divided by the maximum peak, and the resulting ratios showed how much voltage-gated Na^+ (Na_v) channels were inactivated at certain membrane potentials. The half-inactivation is presented in this paper as the membrane potential (I_{Na} Peak/I_{Na} Peak (Max)) = 0.5. This inactivation curve shows the cumulative peak from 23 neurons. Each neuron also had an individual inactivation curve constructed, where their individual membrane potentials at half inactivation values were derived and compared. Two additional inactivation plots were constructed for Top vs. Bottom and Large vs. Small DA neurons, which were taken from the pooled sample of 23 neurons. To derive the amount of time it would take to remove inactivation from 63% of Na_vs, we constructed an interpulse interval (IPI) curve. This curve was derived by depolarizing each neuron with two 20-ms 60 mV voltage steps, with each pair of pulses separated by increasing intervals (0.5, 1, 3, 5, 7.5, 10, 12.5, 15, and 50 ms). At each IPI, the peak of current 2 (from the second 60 mV pulse) was divided by the peak of current 1 (from the first 60 mV pulse). The resulting ratio shows how the increasing durations of IPIs remove the inactivation of Na_v. The amount of time it would take to remove inactivation from 63% of these channels was derived when the curve crossed I_{Na} Peak 2/I_{Na} Peak 1 = 0.63. The cumulative curve was constructed from 25 neurons. Subsequently, each neuron also had its own IPI curve constructed, and their individual times to remove inactivation from 63% of Na_vs were derived and compared. Two additional removal of inactivation plots were constructed for Top vs. Bottom and Large vs. Small DA neurons, which were taken from the pooled sample of 25 neurons.

Ramp protocols

For all analyses involving ramp stimuli, the "ON current" and "OFF current" were found at the beginning and ending of action potential firing, respectively. The interspike period (Δt) was calculated as the time between two consecutive action potentials, with Δt_1 = the time between the

first and second action potential, Δt_2 = the time between the second and third action potential, and so on. Individual spike frequencies (f) were determined by taking the inverse of each Δt.

Data Analysis

For all statistical and graphical analyses, GraphPad Prism (version 8.2.1; La Jolla, CA, USA) was used. All data are presented as mean ± standard error of the mean (SEM). Homogeneity of variance was determined via the F-test. The normality of residuals was checked with the Kolmogorov-Smirnov and Shapiro-Wilk tests. Residuals were considered normally distributed if p-values were > 0.05. Additionally, the residual and Q-Q plots were visualized to confirm residuals' normality. As the sampled distributions had normal distributions and equal variances, unpaired t-tests were used to determine whether mean values for membrane properties differed based on two groups of independent categorical variables – GL localization ("Top" vs. "Bottom" of GL) or neuronal area ("Large" vs. "Small" neurons). These results are presented as t(df) = x.xx, p = 0.xx. Statistically significant values are represented as any p-value less than 0.05. * = p < 0.05; ** = p < 0.01; *** = p < 0.001; **** = p < 0.0001.

For the ramp experiments, we transformed all the results into log-log plots by taking the logarithms of the x-values (ramp slopes) and the y-values (ON/OFF currents, spiking frequencies, and spike numbers). This transformation linearized the data, indicating that they are distributed as power functions, $y = 10^{b} \cdot x^{m}$, where b is the y-intercept and m is the slope of the transformed data. With the data now linearized, we compared the slopes of each group (Top vs. Bottom and Large vs. Small DA neurons) using a simple linear regression analysis, after confirming that the criteria for normality (as described above) were met. A significant difference ($p < 0.05$) in m between different DA groups indicates a significantly different responses to changes in ramp slopes.

Results

Visualization and glomerular localization of rat olfactory bulb dopamine neurons

Most fluorescent OB DA neurons were localized to the GL (**Fig. 1A-C**). Some DA neurons were also expressed in layers deep to the GL, including the EPL, mitral cell layer (MCL), and granule cell layer (GCL) (**Fig. 1B**). Neurons expressed in layers deep to the GL are likely the neonatal and adult-born DA neurons that are migrating from the subventricular zone and rostral migratory

stream to their final destination within the GL (Baker et al., 2001; Betarbet et al., 1996; Pignatelli et al., 2009). Roughly 1,700 TH-positive neurons were previously reported in the EPL (Parrish-Aungst et al., 2007). These OB DA neurons showed a variety of morphologies, including multipolar and bipolar shapes, with varying soma sizes (**Fig. 1B** and **C**). Some areas in the GL have DA neurons that are equally distributed around their respective glomeruli's circumferences (**Fig. 1B** and **C**). We determined whether these neurons express differences that may account for them being more than one OB DA neuron subtype.

Insert Figure 1 around here.

Membrane properties

It is unclear whether the properties of OB DA neurons expressed in the superficial half of the glomerulus (closer to the ONL; "Top," red neurons) differ from those expressed in the deeper half of the glomerulus (closer to the EPL; "Bottom," blue neurons) (**Fig. 2A**). Such differences may be indicative of different neuronal subtypes, such as PGCs and SACs. We compared membrane resistance, capacitance, neuronal areas, time constants, and action potential thresholds between DA neurons localized to the upper/"top" and lower/"bottom" portions of their respective glomeruli. In the following sections, we also compared the properties of ionic currents (I_{Na}, I_H, and ON and OFF currents) and spiking properties (spiking frequencies and number of spikes) between these groups of DA neurons. For this section, we compared the membrane properties of 64 recorded neurons (32 "Top", 32 "Bottom", and 9 neurons not identified by their localization, which were not included in the "Top" vs. "Bottom" analyses) (**Table 1**).

There were no significant differences between Top and Bottom neurons in regard to their membrane resistance ($n = 64$ neurons, $t(62) = 0.8151$, $p = 0.4181$, **Fig. 2Ci**), capacitance ($n = 64$ neurons, $t(62) = 1.050$, $p = 0.2979$, **Fig. 2Di**), neuronal areas ($n = 64$ neurons, $t(62) = 0.1.050$, $p = 0.2979$, **Fig. 2Ei**), time constants ($n = 64$ neurons, $t(62)=0.82$, $p = 0.4153$, **Fig. 2Fi**), and action potential thresholds ($n = 20$ neurons, $t(18) = 1.398$, $p = 0.1792$, **Fig. 2Gi**). Additionally, we observed a wide distribution of neuronal areas for these DA neurons (**Fig. 2H**), which coincides with previous findings that OB DA neuron subtypes may be distinguished by their size (Chand et al., 2015; Galliano et al., 2018; Kosaka et al., 2019; Kosaka and Kosaka, 2009; Pignatelli et al., 2005; Pignatelli and Belluzzi, 2017).

Table 1. Membrane properties of recorded OB DA neurons based on glomerular localization.

	Top of glomerulus	Bottom of glomerulus	All neurons
Membrane resistance (MΩ)	1725 ± 173.5	1926 ± 174.5	1742 ± 113.5
Membrane capacitance (pF)	30.71 ± 1.44	28.64 ± 1.33	29.96 ± 0.95
Neuronal area (μm^2)	3071 ± 144.1	2864 ± 133.4	2996 ± 94.72
Time constant (ms)	48.57 ± 3.82	53.26 ± 4.26	49.27 ± 2.7
Action potential threshold (pA)	325.2 ± 34.80	251.3 ± 40.09	298.7 ± 23.35

All results presented as mean ± SEM, with no significant differences ($p > 0.05$) between Top and Bottom DA neurons. The "All neurons" column includes neurons localized to the top and bottom of the GL and those not initially distinguished by their glomerular localization.

Given the previous findings (Halász et al., 1981; Kosaka and Kosaka, 2007, 2008, 2009; Pignatelli et al., 2005) of differences in soma sizes between two potential populations of OB DA neurons and our finding that neuronal areas of DA neurons are widely distributed (**Fig. 2H**), we also compared these same properties between recorded DA neurons with different sizes (**Table 2**). For these results, we compared neurons classified as "Large" (3390 to 4890 μm^2, n = 24, green neurons) and with neurons classified as "Small" (1589 to 2610 μm^2, n = 24, pink neurons) (**Fig. 2B**). These separations are also marked by dashed lines, with each color corresponding to neuronal size (**Fig. 2H**). The neuronal areas in these groups were significantly different from each other (n = 48 neurons, $t(46) = 16.23$, $p < 0.0001$, **Fig. 2Eii**).

The membrane resistance was significantly greater in Small neurons (n = 48 neurons, $t(46) = 4.251$, $p = 0.0001$, **Fig. 2Cii**), and the capacitance was significantly greater in Large neurons (n = 48 neurons, $t(46) = 16.23$, $p < 0.0001$, **Fig. 2Dii**). These results were expected, because membrane resistance and capacitance are a function of neuronal size (further functional implications are also addressed in the Discussion). There was no significant difference in time constants between Large and Small neurons (n = 48 neurons, $t(46) = 0.1536$. $p = 0.8786$, **Fig. 2Fii**). The action potential thresholds were significantly greater in Large than Small neurons (n = 14 neurons, $t(12) = 5.898$, $p < 0.0001$, **Fig. 2Gii**). These results are summarized in **Table 2**.

Table 2. Membrane properties of recorded OB DA neurons based on neuronal area.

	Large neurons	Small neurons
Membrane resistance (MΩ)	1274 ± 107.9	2401 ± 242.1***
Membrane capacitance (pF)	39.32 ± 0.917****	21.23 ± 0.633
Neuronal area (μm^2)	3932 ± 91.73****	2123 ± 63.27
Time constant (ms)	50.41 ± 4.462	51.50 ± 5.549
Action potential threshold (pA)	417.8 ± 23.99****	181.7 ± 33.51

All data presented as mean ± SEM.

Insert Figure 2 around here.

General action potential spiking properties

All electrophysiology recordings were made in whole-cell current-clamp or voltage-clamp mode. The DA neurons were easily targeted for recording based on their green fluorescence (**Fig. 1**). A total of 140 DA neurons were recorded in horizontal OB slices. The first set of experiments examined whether these neurons display spontaneous, non-synaptically driven action potential firing, which is a well-characterized property of mouse OB DA neurons (Chand et al., 2015; Pignatelli et al., 2005; Puopolo et al., 2005). None of the neurons examined (n = 32) fired spontaneous action potentials (**Fig. 3A**). Many recordings showed evidence of excitatory postsynaptic potentials (EPSPs, the peaks in **Fig. 3A**), indicating the presence of excitatory input to DA neurons, likely from OSNs, M/TCs, and/or ETCs, which may show that these neurons have reached maturity (Pignatelli et al., 2009). Some DA neurons did fire action potentials without stimulation (data not shown); however, these neurons appeared to be synaptically driven, because they did not show firing at a consistent frequency (4-12 Hz) associated with the spontaneous activity of OB DA neurons in mouse OBs (Pignatelli et al., 2005; Puopolo et al., 2005). Therefore, the firing activity of rat OB DA neurons cannot be considered spontaneous, representing a possible functional species difference between rat and mouse OBs.

We further examined the spiking profile of these neurons in response to depolarizing current step stimuli. Of the 60 DA neurons recorded for this activity, 59 neurons displayed single spiking activity at some stimulus level: in response to a sufficiently large depolarizing stimulus, these neurons produced a single action potential, followed by a plateau phase (depolarization block) for the duration of the stimulus (**Fig. 3B**). While these neurons would display single

spiking activity for some stimuli as low as 80 pA (**Fig. 3C**). In contrast, mitral cells would display tonic spiking in response to a much larger 200 pA stimulus (**Fig. 3D**). Thus, the DA neurons may be single spikers. However, of these 59 neurons, 27 neurons additionally produced multiple action potentials in response to weaker depolarizing stimuli (**Fig. 3E** and **F**). As shown in **Fig. 3F**, the multiple spike pattern produced with a weak stimulus (blue) was replaced by decaying spikes and depolarization block at a larger stimulus level (red). With even larger stimuli the cell becomes a single spiker. Therefore, these single spiker neurons are most responsive to weaker stimuli, so that they may act as high-pass filters (Korshunov et al., 2017; also see Discussion).

Further, to analyze whether these spiking properties differ between Top and Bottom and/or Large and Small neurons, we assigned "dummy variables" to add a quantitative measure to these qualitative properties (0 = no more than one spike at any depolarizing stimulus; 1 = multiple spiking only at weaker depolarizing stimuli). After summating these values and comparing the means, there was no significant difference between the spiking properties of DA neurons based on glomerular localization (Top: 0.474 ± 0.117, n = 19; Bottom: 0.529 ± 0.125, n = 17; n = 36 neurons, $t(34) = 0.3249$, $p = 0.7472$, **Fig. 3Gi**), but there was a difference based on the neuronal area of the neuron (Large: 0.6429 ± 0.133, n = 14; Small: 0.154 ± 0.104, n = 13; n = 27, $t(25) = 2.866$, $p = 0.0083$, **Fig. 3Gii**). Therefore, larger DA neurons are more likely to produce multiple spikes in response to weaker depolarizing stimuli than are smaller DA neurons.

Insert Figure 3 around here.

Na^+ current

In whole-cell voltage-clamp, all recorded neurons displayed the fast-activating and inactivating inward I_{Na} (**Fig. 4A**). To isolate the I_{Na} in these neurons, recordings were performed with a 132 mM Cs-based intracellular solution and bath-applied 100 μM Cd (see Materials and Methods). The transient fast activating and inactivating I_{Na} was often no longer than 10 ms (**Fig. 4A**). Recordings from 33 neurons were made for these experiments. The I_{Na} current-voltage curve shows that peak current is largest when the membrane is depolarized to between -20 and 0 mV (n = 11 neurons; **Fig. 4B**).

To visualize the inactivation properties of this current, a I_{Na} h_{∞}-curve (**Fig. 4E**, but also see Materials and Methods) was derived. An example protocol used to derive this curve is included in **Fig. 4C**. The resulting I_{Na} inactivation curve shows half-inactivation at -49 mV (n = 23 neurons; **Fig. 4E**). To determine if these I_{Na} inactivation properties differ between DA neurons based on their localization or neuronal area, an inactivation curve was derived for each neuron, and the individual membrane potentials at 50% I_{Na} inactivation were summated and their means compared. There were no significant differences based on glomerular localization (n = 23 neurons, $t(21) = 1.279$, $p = 0.2149$, **Fig. 4Fi**) or neuronal area (n = 13 neurons, $t(11) = 0.7577$, $p = 0.4654$, **Fig. 4Fii**) of OB DA neurons (**Table 3**). To further determine if this current contributes to the spiking difference seen in **Fig. 3Gii**, we examined and compared the inactivation curves of Top and Bottom (**Fig. 4Gi**) and Large and Small (**Fig. 4Gii**) neurons at membrane potentials of interest (-70 and -60 mV). This comparison was prompted by our observation that spiking differences between Large and Small neurons with weaker current stimuli (closer to their resting potential) would disappear when those stimuli increased in strength. Whereas the inactivation curve for Top neurons was left shifted from that for the Bottom neurons, there were no significant differences between the Top and Bottom inactivation curves at either of the membrane potentials of interest (-70 mV: n = 23 neurons, $t(21) = 1.494$, $p = 0.15$; -60 mV: n = 23 neurons, $t(21) = 1.926$, $p = 0.0677$). Similarly, the inactivation curve for Small neurons was left shifted from that of Large neurons, and there were significant differences at both membrane potentials (-70 mV: n = 13 neurons, $t(11) = 3.748$, $p = 0.0032$; -60 mV: n = 13 neurons, $t(11) = 2.576$, $p = 0.0258$) between Large and Small neurons' inactivation curves. This finding suggests that Small DA neurons' Na_vs are more sensitive to inactivation that Large neurons at membrane potentials close to the resting membrane potential.

Lastly, to characterize the rate of recovery from inactivation, an IPI I_{Na} curve (**Fig. 4H,** but also see Materials and Methods) was derived. An example protocol used to derive this curve is included in **Fig. 4D**. The resulting IPI curve shows that the average time that it takes for 63% of Na_v channels to recover from inactivation (τ) was 13 ms (n = 25 neurons; **Fig. 4H**). Again, to determine if these properties differed between DA neurons based on their localization or neuronal area, an IPI curve was derived for each neuron, and the individual τ values were summated and their means compared. There were no significant differences based on glomerular localization (n = 25 neurons, $t(23) = 0.03674$, $p = 0.9710$, **Fig. 4Ii**) or neuronal area (n = 12

neurons, t(10) = 1.114, p = 0.2913, **Fig. 4Iii**) of these DA neurons (**Table 3**). To further determine if recovery from Na_v channel inactivation influences the spiking difference seen in **Fig. 3Gii**, we constructed and compared IPI curves for Top and Bottom (**Fig. 4Ji**) and Large and Small (**Fig. 4Jii**) neurons. These curves were similar between Top and Bottom and Large and Small neurons throughout increasing IPIs.

Table 3. I_{Na} properties of OB DA neurons.

	Top	Bottom	Large	Small	All
50% I_{Na} inactivation (mV)	-51.16 ± 1.93	--47.59 ± 1.62	-48.27 ± 1.934	-57.16 ± 3.14	-49
IPI (ms)	13.35 ± 1.353	13.41 ± 1.128	14.53 ± 1.633	11.07 ± 2.918	13

All data, except for the "All" category presented as mean ± SEM. There were no significant differences between Top and Bottom DA neurons or between Large and Small DA neurons

Insert Figure 4 around here.

H-current

The I_H (a nonspecific cation current activated during hyperpolarization) is produced by the hyperpolarization-activated cyclic nucleotide-gated (HCN) channels (Biel et al., 2009; Wahl-Schott and Biel, 2009). Because the I_H has been shown to indirectly influence the resting membrane potential of OB DA neurons (Pignatelli et al., 2013), and because it influences several spiking frequencies in the hippocampus (Biel et al., 2009), we analyzed its strength as a possible metric that could contribute to spiking differences between Large and Small DA OB neurons (**Fig. 3Gii**). The presence of I_H in our recordings was identified by depolarizing voltage sags in the membrane potential when a sufficiently large hyperpolarizing current is applied. It can also contribute to rebound spiking after the removal of the hyperpolarizing applied current. Both sag and rebound spiking are exemplified in **Fig. 5A**, confirming that rat OB DA neurons possess I_H. Examples of individual hyperpolarizing traces and the presence of voltage sags are also shown for Top, Bottom, Large, and Small DA neurons (**Fig. 5B**).

The voltage sag ratio (see Materials and Methods for calculation methods), a proxy of the slowly-activating I_H (see Discussion), was used to differentiate between OB DA neurons based on their localization in the GL and neuronal areas. Two sets of voltage sag ratios were used: one

set from voltage traces resulting from a -25-pA stimulus only and the second from traces resulting from some combination of -25, -50, or -75 pA stimuli (or all three). For voltage sags resulting from a -25-pA stimulus only, there was no significant difference between the voltage sag ratios of DA neurons based on glomerular localization (n = 34 neurons, $t(32) = 0.765$, $p = 0.45$, **Fig. 5Ci**), but there was a significant difference based on neuronal area (n = 26 neurons, $t(24) = 3.009$, $p = 0.0061$, **Fig. 5Ciii**) (**Table 4**). Likewise, for voltage sags resulting from the combination of hyperpolarizing stimuli ("all currents" in the figure legend), there was no significant difference between the voltage sag ratios of DA neurons based on localization (n = 26 neurons, $t(24) = 0.5456$, $p = 0.5904$, **Fig. 5Cii**), but there was a significant difference based on neuronal area (n = 18 neurons, $t(16) = 3.113$, $p = 0.0067$, **Fig. 5Civ**) (**Table 4**).

A reason why smaller DA neurons display larger voltage sag ratios, possibly indicating a stronger overall I_H, is due to the large resistance of these neurons. However, Small DA neurons may also possess a larger HCN channel density than Large neurons, which would further contribute to a larger voltage sag ratio in the Small population. To test this hypothesis, we divided the voltage sag ratios into two groups based upon the voltage that they dropped to immediately upon application of the hyperpolarizing applied current (V_i). In one group, the V_i was greater than (positive to) -120 mV, and in the second group V_i was less than (negative to) -120 mV. This division was made since HCN channels are typically almost entirely activated at potentials below -120 mV (Ross et al., 2017), so this second group should have almost maximally-activated channels. If Small neurons possess greater voltage sag ratios than Large neurons at these potentials, then they will likely have a stronger I_H, possibly due to a greater density of HCN channels. When the V_i was positive to -120 mV, the voltage sag ratio did not significantly differ between DA neurons based on their glomerular localization (n = 49 sags, $t(47) = 0.4173$, $p = 0.6784$, **Fig. 5Di**) but the voltage sag ratio was significantly greater in Small versus Large neurons (n = 30 sags, $t(28) = 5.547$, $p < 0.0001$, **Fig. 5Dii**) (**Table 4**). When the V_i was negative to -120 mV, there was again no significant difference in the voltage sag ratio between DA neurons based on their glomerular localization (n = 90 sags, $t(88) = 1.139$, $p = 0.2576$, **Fig. 5Ei**), but the voltage sag ratio was significantly greater in Small versus Large neurons (n = 63 sags, $t(61) = 2.064$, $p = 0.0432$, **Fig. 5Eii**) (**Table 4**). Thus, Small DA neurons possessed a stronger I_H than Large DA neurons, regardless of how the sag ratio quantification was performed.

Table 4. I_H properties of OB DA neurons.

	Top	Bottom	Large	Small
Voltage sag ratio (-25 pA)	0.05 ± 0.01	0.07 ± 0.02	0.03 ± 0.01	0.10 ± 0.05**
Voltage sag ratio (all)	0.06 ± 0.02	0.07 ± 0.02	0.04 ± 0.01	0.12 ± 0.03**
V_i positive to -120 mV	0.03 ± 0.2 x 10^{-2}	0.03 ± 0.3 x 10^{-2}	0.03 ± 0.3 x 10^{-2}	0.10 ± 0.02****
V_i negative to -120 mV	0.07 ± 0.8 x 10^{-2}	0.09 ± 0.01	0.06 ± 0.8 x 10^{-2}	0.10 ± 0.02*

All data presented as mean ± SEM. There were no significant differences between Top and Bottom DA neurons, but there were several significant differences between Large and Small DA neurons.

Insert Figure 5 around here.

Current ramps reveal spiking properties

In the next experiments, we applied ramp stimulus protocols (**Fig. 6A**), where the input current is gradually increased to a peak and is then removed. This protocol was used to avoid or postpone the depolarization block that occurs in OB DA neurons when the input current is applied as a step pulse (**Fig. 3**), allowing analysis of spiking properties of the neurons. The ramp protocols used for the following experiments varied in 6 amplitudes (starting with 0 pA and increasing to either 100, 200, 300, 400, 500, or 600 pA) over 7 durations (50, 100, 200, 300, 400, 500, or 600 ms). In total, 42 ramps were used. The ramps with longer duration and smaller current amplitude have shallow slopes (in pA/ms), so there is a more gradual application of the stimulus, and the ramps with shorter duration and large current amplitudes have steep slopes.

In the first experiment, we examined how the ramp slopes influenced the amount of current required for a neuron to begin spiking ("ON current") and end spiking ("OFF current") (**Fig. 6A**). At the OFF current, a depolarization block is initiated that lasts for the duration of the stimulus. A total of 19 DA neurons were tested, including neurons that produced one or more action potential spike(s) per ramp. Steeper ramp slopes consistently resulted in larger ON and OFF currents in all DA neurons tested (**Fig. 6B**). This result indicates that neurons fire over a longer range of current when stimulated with steep slopes, but their duration of firing decreases with increasing ramp slopes ($\text{Duration} = \left(\frac{\text{OFF current}}{\text{Ramp slope}}\right) - \left(\frac{\text{ON current}}{\text{Ramp slope}}\right)$). The changes in these responses were then compared between DA neurons based on GL localization and neuronal area.

555 The data appear to be distributed as power functions, $y = 10^{b} \cdot x^{m}$, where *b* and *m* are
556 parameters. For this reason, we transformed the data by taking the common logarithm of the x
557 (ramp slope) and y values (ON- or OFF-current, or spike frequency, or number of spikes) and
558 constructing log-log plots (see Materials and Methods and also Supplementary Figures). This
559 linearized the data, confirming the power-law dependence of the data on the ramp slope, and we
560 looked for significant differences in the slopes *m* of the linearized data (this parameter is the
561 exponent of the power function). There were no significant difference in *m* between Top and
562 Bottom neurons in their increasing ON currents (Top: $b = 1.767$, $m = 0.4494$, n = 9 neurons;
563 Bottom: $b = 1.657$, $m = 0.4281$, n = 10 neurons; p = 0.3405, **Supplementary Fig. 1A**) nor in
564 their increasing OFF currents (Top: $b = 2.116$, $m = 0.4359$, n = 9 neurons; Bottom: $b = 1.993$, m
565 = 0.4537, n = 10 neurons; p = 0.5368, **Supplementary Fig. 2A**) with increasing ramp slopes.
566 The raw, un-transformed data are shown in **Fig. 6C**. For the Large and Small DA neurons, there
567 was no difference in *m* between their increasing ON currents with increasing ramp slope (Large:
568 $b = 1.827$, $m = 0.4274$, n = 5 neurons; Small: $b = 1.612$, $m = 0.4210$, n = 5 neurons; p = 0.7680,
569 **Supplementary Fig. 1B**), but there was a significant difference in *m* between the increasing OFF
570 currents of Small and Large DA neurons (Large: $b = 2.194$, $m = 0.4026$, Small: $b = 1.905$, $m =$
571 0.4729; p = 0.0402, **Supplementary Fig. 2B**). The un-transformed data are shown in **Fig. 6D**.
572 These results indicate that the OFF current for Small neurons increases significantly more with
573 increases in the current ramp slope than does the OFF current for Large neurons, however, Large
574 neurons still have larger OFF currents when stimulated with this range of ramp stimuli (see
575 **Supplementary Fig. 2B** and Discussion). There are no significant differences in either ON or
576 OFF currents between Top and Bottom neurons.
577 *Insert Figure 6 around here.*
578 Next, we examined the frequency response of OB DA neurons over a range of input ramp
579 slopes. Spike frequency was calculated for each individual action potential by measuring the
580 time period (Δt) between that action potential and the next one, and taking the reciprocal of the
581 period to determine frequency (*f*) (**Fig. 6A**). This was then averaged over all spikes in the
582 response. A total of 13 neurons that produced more than one action potential per ramp were used
583 for these experiments. Overall, the spike frequency increased with increasing ramp slopes**,** up to
584 a saturation frequency (~70-75 Hz) (**Fig. 7A**). The change in spike frequency was used as
585 another metric to compare DA neurons based on glomerular localization and neuronal area. The

586 *m* for the increase in spike frequency across ramp stimuli did not differ between Top and Bottom
587 DA neurons (Top: *b* = 1.568, *m* = 0.2900, n = 6 neurons; Bottom: *b* = 1.567, *m* = 0.3068, n = 7
588 neurons; p = 0.35, **Supplementary Fig. 3A**). The un-transformed data are shown in **Fig. 7B**.
589 However, the significantly higher *m* in Small neurons indicates that they had a greater increase in
590 spike frequency than Large neurons across increasing ramp slopes (Large: *b* = 1.566, *m* =
591 0.2649, n = 4 neurons; Small: *b* = 1.626, *m* = 0.3217, n = 3 neurons; p = 0.004, **Supplementary**
592 **Fig. 3B**). The un-transformed data are shown in **Fig. 7C**. Thus, Small DA neurons appear to
593 increase their spike frequency with increasing ramp slope strength more than the DA Large
594 neurons.
595 Lastly, we determined the effect of ramp slope on the number of action potentials
596 produced by these neurons. Again, 13 neurons with multiple action potentials per ramp stimulus
597 were used. Overall, the number of action potential spikes decreased with increasing ramp slopes
598 (**Fig. 7D**). We observed differences in this change in the number of action potentials between
599 DA neurons based on both GL localization and neuronal area. Interestingly, Top DA neurons had
600 a significantly more negative *m* than Bottom neurons, and thus produced a greater decrease in
601 spikes across increasing ramp stimuli than Bottom neurons (Top: *b*=0.5636, *m* = -0.3035, n = 6
602 neurons; Bottom: *b* = 0.4046, *m* = -0.1875, n = 7 neurons; p < 0.001, **Supplementary Fig. 4A**).
603 The un-transformed data are shown in **Fig. 7E**. The *m* value was even more significantly
604 negative in Large neurons, indicating that they had an even greater decrease in spikes across
605 increasing ramp stimuli than Small DA neurons (Large: *b* = 0.6208, *m* = -0.3859, n = 4 neurons;
606 Small: *b* = 0.3994, *m* = -0.1909, n = 3 neurons; p < 0.0001, **Supplementary Fig. 4B**). The un-
607 transformed data are shown in **Fig. 7F**.
608 *Insert Figure 7 around here.*
609 These data suggest that slowly increasing inputs result in long, low-frequency responses,
610 while inputs that increase rapidly result in short, high-frequency responses. The number of spikes
611 produced during a current ramp declines faster with the ramp slope in the Top DA neurons than
612 in the Bottom DA neurons. The greatest difference in the number of spikes between these groups
613 appears at shallower ramps (0-7 pA/ms). The Small DA neurons exhibit a greater increase in
614 spike frequency with increase in the current ramp slope than do the Large DA neurons. These
615 same Small DA neurons exhibit less of a decrease in the number of spikes produced as current
616 ramp slope is increased than do the Large DA neurons. We note that the ramp protocol was the

only protocol that we applied that was able to distinguish some differences between Top and Bottom DA neurons.

Discussion

We used a novel transgenic rat line (TH-GFP) to show that DA neurons are widely expressed in the GL of the rat OB. The interneurons that express TH and GABA are collectively termed JGCs, which are among the first neurons to make contact with the OSNs. In the GL, DA, GABA, and glutamate can modulate the odor signal being transmitted to the main output neurons, the M/TCs. These modulatory mechanisms include inhibition of glutamate release from OSNs via presynaptic activation of the D_2 and $GABA_B$ receptors (Baker et al., 1986; Berkowicz and Trombley, 2000; Ennis et al., 2001; Hsia et al., 1999; Nickell et al., 1994; Vaaga et al., 2017), inhibition of glutamate release from M/TCs via D_2 receptor activation (Davila et al., 2003), and an interglomerular inhibition-excitation of ETCs via activation of $GABA_A$ and D_1 receptors, respectively (Liu et al., 2013). While there is much understanding about the synaptic activity of OB DA neurons, it is not fully understood if there are more than one type of OB DA neuron and how these neurons respond to artificial stimuli. Based on our examination of membrane properties, we show that OB DA neurons may be differentiated according to their neuronal area, but not always according to their glomerular localization (whether closer to the ONL or the EPL) in the GL. While most membrane properties could not be differentiated between neurons based on their glomerular localization, responses to ramp stimuli, including the ON and OFF currents and the number of spikes as the ramp slope increased, differed between both Top and Bottom neurons and Large and Small neurons. The spiking profiles of these neurons in response to step stimuli were distinguishable by their neuronal area and sometimes by their glomerular localization. Along with these findings, we conclude by discussing potential species differences between OB DA neurons.

Evidence for and potential identity of at least two types of olfactory bulb dopamine neurons

Previous findings commonly categorize OB DA neurons into two size profiles (Chand et al., 2015; Galliano et al., 2018; Halász et al., 1981; Kosaka et al., 2019; Kosaka and Kosaka, 2007, 2008, 2009, 2011; Pignatelli et al., 2005; Pignatelli and Belluzzi, 2017). It is possible that OB DA neurons with smaller soma sizes that sometimes lack an axon are PGCs (Kosaka and

Kosaka, 2011; Nagayama et al., 2014; Pinching and Powell, 1971), while DA neurons with larger soma sizes and interglomerular projections are SACs (Aungst et al., 2003; Bywalez et al., 2017; Kiyokage et al., 2010). Are these two potentially different populations of OB DA neurons differently localized in the GL? Our membrane properties results indicate that there is no preferred glomerular localization of Large and Small DA neurons. However, a recent study by Galliano et al. (2018) found that large TH+/DA neurons were mostly expressed in the deep glomerulus, at the border of GL/EPL. Interestingly, these large neurons exclusively possessed an axon initial segment (AIS), indicating that these DA neurons are axonic (Galliano et al., 2018). While we have recorded a total of 10 Large DA neurons that were localized to the Bottom of the GL, we also recorded from a total of 15 Large DA neurons that were localized to the Top of the GL. Thus, our data suggest that Large DA neurons are found in both the superficial and deep halves of the glomerulus. While Large DA neurons in the deep GL likely possess an axon, Large neurons in the superficial GL may not possess an axon.

A new study by Kosaka et al. (2019) has further described the OB DA population as belonging to four groups: the Large PGCs with apparent axons, Small PGCs that are either axonic or anaxonic, Transglomerular cells with processes extending up to two or more glomeruli, and the Incrusting cells that extend their processes in the periphery of the glomeruli. These findings, along with our results on the many differences (passive membrane properties, tonic spiking or single action potentials, the I_H, OFF currents, spiking frequency, and number of spikes produced) between the "Large" and "Small" OB DA neurons, support the previous findings that there are at least two types of OB DA neurons. It is also clear that, given that there are new ways of differentiating these neurons based on their dendritic arborizations (Bywalez et al. 2017) and projections of their processes (Kiyokage et al., 2010; Kosaka et al., 2019), further studies to better understand OB DA neurons should focus on their spiking properties.

Spiking properties, ionic currents, and further evidence for at least two types of dopamine neurons in the olfactory bulb

When depolarized by conventional current step stimuli, OB DA neurons overwhelmingly (n = 59/60 neurons) produced a single action potential at the beginning of a strong depolarizing stimulus, before entering a depolarization block for the duration of the stimulus (**Fig. 3B** and **C**). This was in contrast to the tonic spiking produced in mitral cells (**Fig. 3D**). Some (n = 27/59

679 neurons) of these single spikers also produced multiple spikes continuously when stimulated
680 with weaker stimuli only (**Fig. 3E** and **F**). Therefore, we classified these neurons as single
681 spikers that are more responsive to weaker stimuli. These neurons may fit the criteria of the "non
682 accommodating" spiking group characterized by McQuiston and Katz (2001), because when they
683 produced tonic spiking, these spikes appeared to maintain a consistent spike frequency
684 throughout the step stimulus. Based on the number of Large and Small neurons that showed
685 these properties, it was more likely that Large OB DA neurons would produce multiple spikes at
686 weaker stimuli, but not Small neurons (**Fig. 3G**). The spiking data imply that the larger OB DA
687 neurons are more responsive to weaker, not stronger, odor stimuli.
688 To examine the role that ionic currents play in these neurons being single spikers, we
689 investigated the I_{Na} (**Fig. 4**). Of these ionic properties, we found that Small DA neurons' Na_V
690 channels were much more sensitive to inactivation at membrane potentials close to the resting
691 membrane potential (-70 mV and -60 mV) than those of Large DA neurons (**Fig. 4Gii**). Thus,
692 this difference in Na_V sensitivity should, at least partially, address the difference in spiking
693 between Large and Small DA neurons (**Fig. 3Gii**). Future studies that could address this
694 difference in spiking could include investigating a potential difference in the density of Na_v
695 between Large and Small DA neurons (Sengupta et al., 2013; Zengel et al., 1985), the neuronal
696 localization of these channels (Kress and Mennerick, 2009; Trimmer and Rhodes, 2004), and
697 further analyses of K^+ currents, including the A-type (Iseppe et al., 2016) and M-currents (Li et
698 al., 2015; Nai et al., 2011). Our reported time constant (13 ms, **Fig. 4H**) is similar to the
699 previously reported 16.8 ms in OB PGCs (Iseppe et al., 2016). In OB PGCs, it was determined
700 that the long time constant required to remove inactivation from Na_V and the short time constant
701 required to remove the inactivation from channels that produce the K^+ A-current contribute to the
702 single spiking properties of OB PGCs (Iseppe et al., 2016). Given our reported values for
703 inactivation and the similarly long removal of inactivation time constant for Na_V, these
704 properties may contribute to the single spiking activity of OB DA neurons.
705 The I_H can act as a pacemaker current for neurons that experience spontaneous, rhythmic
706 spiking (Wahl-Schott, 2009). In mouse OB DA neurons, pharmacological blockade of I_H/HCN
707 did hyperpolarize their resting membrane potential, but this did not cause these neurons to stop
708 their spontaneous spiking (Pignatelli et al., 2013). We did not test the importance of the I_H in the
709 firing properties of rat OB DA neurons. However, as the neurons in our study did not produce

spontaneous spikes (**Fig. 3A**), it is likely that this current does not act as a pacemaker in rat OB DA neurons either. We observed further biophysical difference between Large and Small OB DA neurons in the form of the I_H. The presence of I_H in these neurons was evident, because they produced voltage sags when a hyperpolarizing current was applied, often followed by rebound action potentials that can be due in part to I_H (**Fig. 5A**). We used the voltage sag ratio as a representative measure of the strength of I_H and as a means to distinguish between potential types of OB DA neurons. At all hyperpolarizing stimuli, voltage sag ratios did not differ between DA neurons based on GL localization, but were consistently larger in Small compared with Large DA neurons (**Fig. 5Ciii** and **iv, 5Dii**, and **5Eii**). One functional implication of I_H could be that it allows for the smaller neurons to get out of hyperpolarization, bypass their action potential thresholds (which would be easier for these neurons since smaller neurons have a lower threshold, **Fig. 2Gii**), and generate an action potential earlier than larger neurons. Given the inactivation properties of Na_vs in Small neurons, their larger I_H can indirectly inactivate these channels more than it would in Large DA neurons, which may contribute to the difference in spiking between these neurons.

According to Ohm's Law, smaller neurons should produce a greater voltage drop when hyperpolarized than larger neurons, activating a larger fraction of HCN channels. Thus, smaller neurons would be expected to produce larger voltage sags, as well. However, if larger DA neurons experienced the same voltage drop as smaller neurons, would their voltage sag ratios be different or the same? As we found that Small DA neurons experienced larger voltage sag ratios even when they began at similar membrane potentials as Large DA neurons (**Fig. 5D-E**), we conclude that Small DA neurons have a stronger I_H than Large neurons. Interestingly, the difference in voltage sag ratios between Small and Large neurons was much greater at more positive hyperpolarized potentials (**Fig. 5D**) than more negative hyperpolarized potentials (**Fig. 5E**). This suggests that the HCN channel activation curve could be right shifted in the smaller neurons, so that the channels activate at higher voltages.

It should be noted that, while some of the recorded neurons did not have noticeable voltage sags, it does not necessarily mean that they do not possess an I_H. Depending on the presence of specific HCN subunits (subunits 1-4; Meredith et al., 2012; Wahl-Schott and Biel, 2009), these neurons may possess the fast-activating I_H, slow-activating I_H, or a mixture of both. The fast-activating I_H rapidly opposes the applied hyperpolarizing current, reducing the size of

the voltage drop when the hyperpolarizing current is applied. In contrast, the slow-activating I_H produces the voltage sags (Ross et al., 2017). Therefore, those neurons that did not display voltage sags (a property of slow-activating I_H) may still possess the fast-activating I_H. Future experiments could label the HCN subunits and verify the distribution of the fast and slow components of the I_H among different rat OB DA neurons, as has recently been done in vestibular ganglion neurons (Michel et al., 2015).

Further spiking properties in response to current ramp stimulations

Our current clamp data up to this point show spiking in response to single step stimuli. While current step protocols provide a good snapshot of the spiking response per individual stimulus, we wanted to further characterize spiking properties in response to increasing stimuli. Thus, we used ramp stimuli, which can be thought of as a new current step stimulus every millisecond. Ramps with smaller current amplitudes and longer durations had shallow slopes, while ramps with larger amplitudes and shorter duration had steep slopes ("ramp slopes" is interchangeable with "ramp stimuli"). The resulting power functions (**Figs. 6** and **7**) and their transformed log-log plots (Materials and Methods and Supplementary Figures) describe the response of these neurons to increasing ramp stimuli, as well as differences between the responses of Top vs. Bottom and Large vs. Small DA neurons.

Shallow ramp stimuli yielded smaller ON/OFF currents, while steeper stimuli yielded larger ON/OFF currents (**Fig. 6B**). Shallow ramp stimuli also yielded smaller spike frequencies (**Fig. 7A**) and more spikes (**Fig. 7D**) than steep stimuli. Large neurons produced larger OFF currents than Small neurons (**Fig. 6D**). This is consistent with data in **Fig. 3Gii**, because Large neurons would take a longer time to enter depolarization block than Small neurons, especially at very shallow ramp stimuli (Duration = Current/Ramp slope). Small neurons developed larger spike frequencies across increasing ramp stimuli (**Fig. 7C**) and had considerably fewer spikes at shallow ramp stimuli (**Fig. 7F**) than Large neurons. This again confirms our findings that not only are OB DA neurons more sensitive to weaker stimuli, but Large DA neurons tend to develop more, lower interspike frequency action potentials than Small neurons. While these results confirm our hypothesis for Large and Small neurons based on **Fig. 3**, the findings between Top and Bottom neurons are less intuitive.

There are two parameters – derived from log-log plots – that influence these DA neurons: 10^b and x^m. Whereas 10^b is a constant, x^m changes with increasing ramp stimuli. If the exponent *m* (which is the slope of the linear equations generated in log-log plots, and also the exponent of the ramp slope stimulus in the un-transformed power functions) is significantly greater in one group, then the change that group experiences will increase (or decrease, if *m* is negative) more than the other group. Small neurons experience a greater increase in their spike frequencies (**Supplementary Fig. 3B**), with a smaller decrease in their overall spiking (**Supplementary Fig. 4B**), compared to Large neurons as ramp stimuli increase. Small neurons also have a significantly larger increase in their OFF currents than Large neurons with increasing ramp stimuli, as demonstrated by their greater *m* value (**Supplementary Fig. 2B**). However, because the *b* value for Small neurons (1.905) is smaller than that of the Large neurons (2.194), the OFF current for Large neurons will consistently stay higher than that of Small neurons across the ramp stimuli that we tested (0-12 pA/ms) and is consistent with the data presented here that Large neurons have a longer duration of spiking than Small neurons. This means that the constant 10^b also dictates the spiking properties of not only Large and Small neurons, but also those of Top and Bottom neurons (**Figs. 6C** and **7E**). Some of the properties that can contribute to the *b* and *m* parameters of each neuron include that neuron's action potential threshold (rheobase – **Fig. 3G**), I_{Na} properties, including inactivation (**Fig. 4E** and **G**), Na_v density (Sengupta et al., 2013; Zengel et al., 1985) and distribution throughout the neuron (Kress and Mennerick, 2009; Trimmer and Rhodes, 2004), K^+ current properties, including the fast-activating and inactivating A-type current (Iseppe et al., 2016) and the non-inactivating M-current (Li et al., 2015, Nai et al., 2011), the I_H (**Fig. 5** and Pignatelli et al., 2013), and further biophysical properties. Some of the differences between Top and Bottom neurons may also come from morphological properties, including possessing an axon/AIS (Chand et al., 2015; Galliano et al., 2018) and the growing classification of DA neurons in the OB (Kosaka et al., 2019), among other factors.

Do olfactory bulb dopamine neurons act as high-pass filters?

Which spiking pattern is more effective at releasing neurotransmitter depends on the presynaptic plasticity that occurs in the DA neuron's presynaptic terminals. If the synapses facilitate, then high-frequency bursts of activity are likely more effective. However, if depletion of the readily

802 releasable vesicle pool predominates, then the low-frequency spike trains could be more
803 effective. The efficacy of the response of DA neurons to ramp input thus raises several questions.
804 Are OB DA neurons dependent on action potentials for DA release, and what are the most
805 effective stimuli for inducing transmitter release from these OB DA neurons? How can these
806 gating mechanisms contribute to functionality of OB DA neurons?
807 First, because OB DA release can be evoked by a single action potential (Borisovska et
808 al., 2013), OB DA neurons receive excitatory synaptic input (Hayar et al., 2004), and their
809 synaptic activity increases after depolarization (Baker et al., 1986; Berkowicz and Trombley,
810 2000; Davila et al., 2003; Ennis et al., 2001; Hsia et al., 1999; Liu et al., 2013; Nickell et al.,
811 1994; Vaaga et al., 2017), it is likely that exocytosis of synaptic vesicles is triggered by electrical
812 impulses. These levels of release would likely differ depending on the time of the day, with
813 higher levels in the daytime and lower levels in the nighttime of rodents (Corthell et al., 2013).
814 Unlike the midbrain DA neurons (Covey et al., 2016; Ito and Schuman, 2007; Suaud-
815 Chagny, 2004; Suaud-Chagny et al., 1992; Zhang et al., 2009; Zhang and Sulzer, 2004), to the
816 best of our knowledge, there is no direct evidence to suggest that OB DA neurons are more
817 sensitive to stronger stimuli. Rather our data combined with the functionality of these neurons
818 provide support for the notion that they are more sensitive to weaker stimuli. Because OB DA
819 neurons are inhibitory, they may filter out the background, tonic odors. In the context of the OB,
820 this suggests that DA neurons may act as high-pass filters to allow stronger odor signals to be
821 processed by the main output neurons (Korshunov et al., 2017). A similar hypothesis was
822 described for the function of calretinin PGCs, which are also single spikers (Iseppe et al., 2016).
823 Whether DA neurons may act as high-pass filters depends on whether these neurons stop
824 releasing transmitter during depolarization block. When these neurons receive a large enough
825 stimulus, they will revert to inactivity, which is characterized by depolarization block (plateau,
826 non-spiking phase that can be distinguished in **Fig. 3B**, **C**, and **F**). Does this inactivity mean that
827 OB DA neurons can no longer be synaptically active? During depolarization block, these
828 neurons have a depolarized membrane potential of about -40 to -30 mV. This depolarization
829 could activate Ca_v channels that are necessary for inducing a synaptic cascade, thus releasing DA
830 and GABA. If this is the case, then these neurons can still be synaptically active, even though
831 they are quiescent in terms of their somatic action potentials. This would especially be likely if a
832 somatic action potential/depolarization block is proximal to the Ca_v of dendrites, causing a

dendritic release of transmitters. However, depolarization block causing transmitter release may not be as likely for DA neurons expressing an axon. Without somatic action potentials, saltatory conduction in the nodes of Ranvier of the axon may not be possible. If saltatory conduction still occurs during depolarization block, then we would expect to record back-propagating action potentials during depolarization block. Additionally, a simulated study shows that high-frequency stimulations of axons will cause partial depolarization block (Guo et al., 2018). Therefore, since there is/are a subpopulation of OB DA neurons that do express an axon (Galliano et al., 2018; Kosaka et al., 2019), and because DAergic projections can span up to 1 mm (Kiyokage et al., 2010), it is unlikely that sustained depolarization block will cause synaptic release at the axonal terminals of a subset of OB DA neurons. Future voltammetry studies, which can measure DA release from dendrites and axon terminals, while simultaneously recording depolarization block in soma, may be an effective approach for answering this question.

In the OB, DA release causes a presynaptic inhibition of OSNs via the D_2 receptor, effectively decreasing excitatory input onto and from the M/TCs (Berkowicz and Trombley, 2000; Davila et al., 2003; Ennis et al., 2001; Hsia et al., 1999; Liu et al., 2013; Nickell et al., 1994; Vaaga et al., 2017). Perhaps, higher odor concentrations could inhibit DA neurons, as did the stronger depolarization stimuli (**Fig. 3E** and **F**) and steeper ramps (**Fig. 7D, E,** and **F**). If these stronger odors bypass the DAergic network in the glomerulus, then these neurons may act as high-pass filters (Korshunov et al., 2017): actively inhibiting transmission of weak/ambient odors while being quiescent in the presence of stronger odors. Thus, the activity of OB DA neurons may increase odor discrimination through the D_2 receptor (Tillerson et al., 2006) by inhibiting glutamate release from its intraglomerular OSNs and M/TCs, while having more complicated, temporal effects on its interglomerular targets (Liu et al., 2013).

Clinical implications

The increasing availability of transgenic mice over the past few decades has caused mice to assume a greater role in biomedical science compared to rats. However, the advent of transgenic rats such as this hTH-GFP rat line (Iacovitti, et al., 2014) allows for further characterization of OB DA neurons from a different rodent species. This adds to the collective knowledge of the function of OB DA neurons, as well as how these neurons may be affected by neurodegenerative diseases such as Parkinson's disease (PD), and is of particular interest to those in the fields of

pathology and neurology. When afflicted with PD, the OB DA neurons of rats and people paradoxically increase in number (Huisman et al., 2004; Lelan et al., 2011; Mundiñano et al., 2011). A loss of olfaction – hyposmia and anosmia – precedes overt PD and can be a sign of the early stages of this disease (Berendse et al., 2001; Doty et al., 1988; Huisman et al., 2004; Ross et al., 2008; Ponsen et al., 2004). This hyposmia and anosmia is possibly due to increased inhibition from the greater number of DA-GABA neurons present in the affected OBs of PD patients (Alizadeh et al., 2015). In some rodent models of PD, rats (but not mice) appear to display Parkinsonian motor deficits more akin to the symptomology in humans (Ellenbroek and Youn, 2016). Our finding that OB DA neurons do not spontaneously spike in rats (**Fig. 3A**), while they do in mice (Pignatelli, et al., 2005; Puopolo, et al., 2005), suggest biophysical differences that may be important in the function of the neurons in odor discrimination. Therefore, clarifying the function of DA neurons in mammalian, including human, OBs and investigating potential species differences may facilitate the successful design of clinical trials and treatments for olfactory dysfunction as well as the early detection of neurodegenerative disorders.

Author Contributions

KSK, LJB, RB, and PQT designed the experiments. KSK performed the experiments and collected data. KSK, LJB, RB, and PQT analyzed the data. KSK wrote the first draft of the manuscript. All authors contributed to subsequent drafts.

Acknowledgement

We thank Charles Badland for his help and guidance with the figures and Dr. Scott Burgess for his discussion and help with statistics. This research was supported by the FSU Chemical Senses Training (CTP) Grant Award T32 DC000044 from the National Institutes of Health (NIH/NIDCD) and by the National Science Foundation (NSF) grant DMS 1853342 to R. Bertram.

Conflict of Interest

The authors have no conflicts of interest to declare.

References

Alizadeh, R., Hassanzadeh, G., Soleimani, M., Joghataei, M.T., Siavashi, V., Khorgami, Z., et al. (2015). Gender and age related changes in number of dopaminergic neurons in adult human olfactory bulb. *J. Chem. Neuroanat.* 69: 1-6. doi: 10.1016/j.jchemneu.2015.07.003.

Aungst, J.L., Heyward, P.M., Puche, A.C., Karnup, S.V., Hayar, A., Szabo, G., et al. (2003). Centre-surrounding inhibition among olfactory bulb glomeruli. *Nature.* 426(6967): 623-629. doi: 10.1038/nature02185.

Bardoni, R., Magherini, P.C., and Belluzzi, O. (1996a). Excitatory synapses in the glomerular triad of frog olfactory bulb in vitro. *Neuroreport.* 7(11): 1851-1855. doi: 10.1097/00001756-199607290-00033.

Bardoni, R., Puopolo, M., Magherini, P.C., and Belluzzi, O. (1996b). Potassium currents in periglomerular cells of frog olfactory bulb in vitro. *Neurosci. Lett.* 210(2): 95-98. doi: 10.1016/0304-3940(96)12677-x.

Baker, H. (1986). Species differences in the distribution of substance P and tyrosine hydroxylase immunoreactivity in the olfactory bulb. *J. Compt. Neurol.* 252: 206-226. doi: 10.1002/cne.902520206.

Baker, H., Liu, N., Chun, H.S., Saino, S., Berlin, R., Volpe, et al. (2001). Phenotypic differentiation during migration of dopaminergic progenitor cells to the olfactory bulb. *J. Neurosci*. 21(21): 8505-8513. doi: 10.1523/JNEUROSCI.21-21-08505.2001.

Baker, H., Towle, A.C., and Margolis, F.L. (1988). Differential afferent regulation of dopaminergic and GABAergic neurons in the mouse main olfactory bulb. *Brain. Res.* 450: 69-80. doi: 10.1016/0006-8993(88)91545-4.

Berendse, H.W., Booij, J., Francot, C.M.J.E., Bergmans, P.L.M., Hijman, R., Stoof, J.C., et al. (2001). Subclinical dopaminergic dysfunction in asymptomatic Parkinson's disease patients' relatives with a decreased sense of smell. *Ann. Neurol.* 50(1): 34-41. doi: 10.1002/ana.1049.

Berkowicz, D.A., and Trombley, P.Q. (2000). Dopaminergic modulation at the olfactory nerve synapse. *Brain. Res.* 855: 90-99. doi: 10.1016/s0006-8993(99)02342-2.

924 Berkowicz, D.A., Trombley, P.Q., and Shepherd, G.M. (1994). Evidence for glutamate as the
925 olfactory receptor cell neurotransmitter. *J. Neurophysiol*. 71: 2557-2561. doi:
926 10.1152/jn.1994.71.6.2557.
927 Betarbet, R., Zigova, T., Bakay, R.A., and Luskin, M.B. (1996). Dopaminergic and GABAergic
928 interneurons of the olfactory bulb are derived from the neonatal subventricular zone. *Int.*
929 *J. Dev. Neurosci*. 14(7-8): 921-930. doi: 10.1016/s0736-5748(96)00066-4.
930 Biel, M., Wahl-Schott, C., Michalakis, S., and Zong, X. (2009). Hyperpolarization-activated
931 cation channels: From genes to function. *Physiol. Rev.* 89: 847-885. doi:
932 10.1152/physrev.00029.2008.
933 Blakemore, L.J., Resasco, M., Mercado, M.A., and Trombley, P.Q. (2006). Evidence for Ca(2+)-
934 permeable AMPA receptors in the olfactory bulb. *Am. J. Physiol. Cell. Physiol.* 290:
935 C925-935. doi: 10.1152/ajpcell.00392.2005.
936 Borisovska, M., Bensen, A.L., Chong, G., and Westbrook, G.L. (2013). Distinct modes of
937 dopamine and GABA release in dual transmitter neuron. *J. Neurosci.* 33(5): 1790-1796.
938 doi: 10.1523/JNEUROSCI.4342-12.2013.
939 Bywalez, W. G., Ona-Jodar, T., Lukas, M., Ninkovic, J., and Egger, V. (2017). Dendritic
940 arborization patterns of small juxtaglomerular cell subtypes within the rodent olfactory
941 bulb. *Front. Neuroanat.* 10: 127. doi: 10.3389/fnana.2016.00127.
942 Cave, J.W., and Baker, H. (2009). Dopamine systems in the forebrain. *Adv. Exp. Med. Biol.* 651:
943 15-35. doi: 10.1007/978-1-4419-0322-8_2.
944 Chand, A.N., Galliano, E., Chesters, R.A., and Grubb, M.S. (2015). A distinct subtype of
945 dopaminergic interneuron displays inverted structural plasticity at the axon initial
946 segment. *J. Neurosci.* 35(4): 1573-1590. doi: 10.1523/JNEUROSCI.3515-14.2015.
947 Cockerham, R., Liu, S., Cachope, R., Kiyokage, E., Cheer, J. F., Shipley, M. T., et al. (2016).
948 Subsecond regulation of synaptically released dopamine by COMT in the olfactory bulb.
949 *J. Neurosci.* 36(29): 7779-7785. doi: 10.1523/JNEUROSCI.0658-16.2016.
950 Corthell, J.T., Stathopoulos, A.M., Watson, C.C., Bertram, R., and Trombley, P.Q. (2013).
951 Olfactory bulb monoamine concentrations vary with time of day. *Neuroscience.* 247:
952 234-241. doi: 10.1016/j.neuroscience.2013.05.040.
953 Covey, D.P., Bunner, K.D., Schuweiler, D.R., Cheer, J.F., and Garris, P.A. (2016).
954 Amphetamine elevates nucleus accumbens dopamine via an action potential-dependent

mechanism that is modulated by endocannabinoids. *Eur. J. Neurosci.* 43(12): 1661-1673. doi: 10.1111/ejn.13248.

Davila, N.G., Blakemore, L.B., and Trombley, P.Q. (2003). Dopamine modulates synaptic transmission between rat olfactory bulb neurons in culture. *J. Neurophysiol*. 90(1): 395-404. doi: 10.1152/jn.01058.2002.

Doty, R.L., Deems, D.A., and Stellar, S. (1988). Olfactory dysfunction in Parkinsonism: A general deficit unrelated to neurologic signs, disease stage, or disease duration. *Neurology.* 38: 1237-1244. doi: 10.1212/WNL.38.8.1237.

Ellenbroek, B., and Youn, J. (2016). Rodent models in neuroscience research: is it a rat race? *Dis. Model. Mech.* 9(10): 1079-1087. doi: 10.1242/dmm.026120.

Ennis, M., Zhou, F.M., Ciombor, K.J., Aroniadou-Anderjaska, V., Hayar, A., Borrelli, E., et al. (2001). Dopamine D2 receptor-mediated presynaptic inhibition of olfactory nerve terminals. *J. Neurophysiol.* 86(6): 2986-2997. doi: 10.1152/jn.2001.86.6.2986.

Ennis, M., Zimmer, L.A., and Shipley, M.T. (1996). Olfactory nerve stimulation activates rat mitral cells via NMDA and non-NMDA receptors in vitro. *Neuroreport.* 7(5): 989-992. doi: 10.1097/00001756-199604100-00007.

Gall, C.M., Hendry, S.H., Seroogy, K.B., Jones, E.G., and Haycock, J.W. (1987). Evidence for coexistence of GABA and dopamine in neurons of the rat olfactory bulb. *J. Comp. Neurol*. 266: 307-318. doi: 10.1002/cne.902660302.

Galliano, E., Franzoni, E., Breton, M., Chand, A.N., Byrne, D.J., Murthy, V.N., et al. (2018). Embryonic and postnatal neurogenesis produce functionally distinct subclasses of dopaminergic neuron. *Elife.* 7: e32373doi: 10.7554/eLife.32373.

Gentet, L.J., Stuart, G.J., and Clements, J.D. (2000). Direct measurement of specific membrane capacitance in neurons. *Biophys. J.* 79(1): 314-320. doi: 10.1016/S0006-3495(00)76293-X.

Golgi C. (1875). Sulla fina struttura dei bulbi olfactorii (On the fine structure of the olfactory bulb). *Riv. Sper. Freniatr. Med. Leg.* 1: 404-425.

Guo, Z, Feng, Z., Wang, Y., and Wei, X. (2018). Simulation study of intermittent axonal block and desynchronization effect induced by high-frequency stimulation of electrical pulses. *Front. Neurosci.* 12: 858. doi: 10.3389/fnins.2018.00858.

985 Halász, N., Johansson, O., Hökfelt, T., Ljunghahl, A., and Goldstein, A. (1981).
986 Immunohistochemical identification of two types of dopamine neuron in the rat olfactory
987 bulb as seen by serial sectioning. *J. Neurocytol*. 10(2): 251-259. doi:
988 10.1007/bf01257970.
989 Hayar, A., Karnup, S., Ennis, M., and Shipley, M.T. (2004). External tufted cells: a major
990 excitatory element that coordinates glomerular activity. *J. Neurosci.* 24(30): 6676-6685.
991 doi: 10.1523/JNEUROSCI.1367-04.2004.
992 Hodgkin, A.L., and Huxley, A.F. (1952). A quantitative description of membrane currents and its
993 application to conduction and excitation in nerve. *J. Physiol.* 117: 500-544. doi:
994 10.1113/jphysiol.1952.sp004764.
995 Holohean, A.M., Rodriguez, C.A., Hackman, J.C., and Davidoff, R.A. (1996). Voltage-gated
996 calcium currents in whole-cell patch-clamped bullfrog dorsal root ganglion cells: effects
997 of cell size and intracellular solutions. *Brain. Res.* 711(1-2): 138-145. doi: 10.1016/0006-
998 8993(95)01414-4.
999 Hsia, A.Y., Vincent, J.D., and Lledo, P.M. (1999). Dopamine depresses synaptic inputs into the
1000 olfactory bulb. *J. Neurophysiol.* 82(2): 1082-1085. doi: 10.1152/jn.1999.82.2.1082.
1001 Huisman, E., Uylings, H.B.M., and Hoogland, P.V. (2004). A 100% increase of dopaminergic
1002 cells in the olfactory bulb may explain hyposmia in Parkinson's disease. *Mov. Dis.* 19:
1003 687-692. doi: 10.1002/mds.10713.
1004 Iacovitti, L., Wei, X., Cai, J., Kostuk, E.W., Lin, R., Gorodinsky, A., et al. (2014). The hTH-GFP
1005 reporter rat model for the study of Parkinson's disease. *PLoS. ONE.* 9(12): e113151. doi:
1006 10.1371/journal.pone.0113151.
1007 Iseppe, A.F., Pignatelli, A., and Belluzzi, O. (2016). Calretinin-periglomerular interneurons in
1008 mice olfactory bulb: cells of few words. *Front. Cell. Neurosci*. 10(231): 1-13. doi:
1009 10.3389/fncel.2016.00231.
1010 Ito, H.T., and Schuman, E.M. (2007). Frequency-dependent gating of synaptic transmission and
1011 plasticity by dopamine. *Front. Neural. Circuits.* 1(1): 1. doi: 10.3389/neuro.04.001.2007.
1012 Keller, A., Yagodin, S., Araniadou-Anderjaska, V., Zimmer, L.A., Ennis, M., Sheppard, N.F. Jr.,
1013 et al. (1998). Functional organization of rat olfactory bulb glomeruli revealed by optical
1014 imaging. *J. Neurosci.* 18(7): 2602-2612. doi: 10.1523/JNEUROSCI.18-07-02602.1998.

Kiyokage, E., Pan, Y.Z., Shao, Z., Kobayashi, K., Szabo, G., Yanagawa, Y., et al. (2010). Molecular identity of periglomerular and short axon cells. *J. Neurosci.* 30(3): 1185-1196. doi: 10.1523/JNEUROSCI.3497-09.2010.

Korshunov, K. S., Blakemore, L. J., and Trombley, P. Q. (2017). Dopamine: A modulator of circadian rhythms in the central nervous system. *Front. Cell. Neurosci.* 11: 91. doi: 10.3389/fncel.2017.00091.

Kosaka, K., Aika, Y., Toida, K., Heizmann, C.W., Hunziker, W., Jacobowitz, D.M., et al. (1995). Chemically defined neuron groups and their subpopulations in the glomerular layer of the rat main olfactory bulb. *Neurosci. Res.* 23: 73-88.

Kosaka, K., Hama, K., Nagatsu, I., Wu, J.Y., Ottersen, O.P., Storm-Mathisen, J., et al. (1987). Postnatal development of neurons containing both catecholaminergic and GABAergic traits in the rat main olfactory bulb. *Brain. Res.* 403(2): 355-360. doi: 10.1016/0006-8993(87)90075-8.

Kosaka, K., and Kosaka, T. (2004). Organization of the main olfactory bulbs of some mammals: musk shrews, moles, hedgehogs, tree shrews, bats, mice, and rats. *J. Comp. Neurol.*472: 1-12. doi: 10.1002/cne.20004.

Kosaka, K., and Kosaka, T. (2005). Synaptic organization of the glomerulus in the main olfactory bulb: Compartments of the glomerulus and heterogeneity of periglomerular cells. *Anat. Sci. Int.* 80(2): 80-90. doi: 10.1111/j.1447-073x.2005.00092.x.

Kosaka, K., and Kosaka, T. (2007). Chemical properties of type 1 and type 2 periglomerular cells in the mouse olfactory bulb are different from those in the rat olfactory bulb. *Brain. Res*. 1167: 42-55. doi: 10.1016/j.brainres.2007.04.087.

Kosaka, K., Toida, K., Aika, Y., and Kosaka, T. (1998). How simple is the organization of the olfactory glomerulus?: the heterogeneity of so-called periglomerular cells. *Neurosci. Res.* 30: 101-110. doi: 10.1016/s0168-0102(98)00002-9.

Kosaka, K., Toida, K., Margolis, F.L., and Kosaka, T. (1997). Chemically defined neuron group groups and their subpopulations in the glomerular layer of the rat main olfactory bulb – II. Prominent differences in the intraglomerular dendritic arborization and their relationship to olfactory nerve terminals. *Neuroscience*. 76(3): 775-786. doi: 10.1016/s0306-4522(96)00308-9.

Kosaka, T., Hataguchi, Y., Hama, K., Nagatsu, I., and Wu, J.Y. (1985). Coexistence of immunoreactivities for glutamate decarboxylase and tyrosine hydroxylase in some neurons in the periglomerular region of the rat main olfactory bulb: possible coexistence of gamma-aminobutyric acid (GABA) and dopamine. *Brain. Res.* 343: 166-171. doi: 10.1016/0006-8993(85)91172-2.

Kosaka, T., and Kosaka, K. (2008). Tyrosine hydroxylase-positive GABAergic juxtaglomerular neurons are the main source of the interglomerular connections in the mouse main olfactory bulb. *Neurosci. Res.* 60(3): 349-354. doi: 10.1016/j.neures.2007.11.012.

Kosaka, T., and Kosaka, K. (2009). Two types of tyrosine hydroxylase positive GABAergic juxtaglomerular neurons in the mouse main olfactory bulb are different in their time of origin. *Neurosci. Res.* 64: 436-441. doi: 10.1016/j.neures.2009.04.018.

Kosaka, T., and Kosaka, K. (2011). "Interneurons" in the olfactory bulb revisited. *Neurosci. Res.* 69: 93-99. doi: 10.1016/j.neures.2010.10.002.

Kosaka, T., and Kosaka, K. (2016). Neuronal organization of the main olfactory bulb revisited. *Anat. Sci. Int*. 91: 115-127. doi: 10.1007/s12565-015-0309-7.

Kosaka, T., Pignatelli, A., and Kosaka, K. (2019). Heterogeneity of tyrosine hydroxylase expressing neurons in the main olfactory bulb. *Neurosci. Res.* In press. doi: 10.1016/j.neures.2019.10.004.

Kress, G.J., and Mennerick, S. (2009). Action potential initiation and propagation: Upstream influences on neurotransmission. *Neuroscience.* 158: 211-222. doi: 10.1016/j.neuroscience.2008.03.021.

Lelan, F., Boyer, C., Thinard, R., Remy, S., Usal, C., Tesson, L., et al. (2011). Effects of human alpha-synuclein A53T-A30P mutations on SVZ and local olfactory bulb cell proliferation in a transgenic rat model of Parkinson's disease. *Parkinsons. Dis.* 2011: 987084. doi: 10.4061/2011/987084.

Li, G., Linster, C., and Cleland, T. A. (2015). Functional differentiation of cholinergic and noradrenergic modulation in a biophysical model of olfactory bulb granule cells. *J. Neurophysiol.* 114: 3177-3200. doi: 10.1152./jn.00324.2015.

Liu, S., Plachez, C., Shao, Z., Puche, A., and Shipley, M.T. (2013). Olfactory bulb short axon cell release of GABA and dopamine produces a temporally biphasic inhibition-excitation

response in external tufted cells. *J. Neurosci.* 33(7): 2916-2926. doi: 10.1523/JNEUROSCI.3607-12.2013.

Liu, S., Puche, A.C., and Shipley, M.T. (2016). The interglomerular circuit potently inhibits olfactory bulb output neurons by both direct and indirect pathways. *J. Neurosci*. 36(37): 9604-9617. doi: 10.1523/JNEUROSCI.1763-16.2016.

Maher, B.J., and Westbrook, G.L. (2008). Co-transmission of dopamine and GABA in periglomerular cells. *J. Neurophysiol.* 99: 1559-1564. doi: 10.1152/jn.00636.2007.

McLean, J. H., and Shipley, M. T. (1988). Postmitotic, postmigrational expression of tyrosine hydroxylase in olfactory bulb dopaminergic neurons. *J. Neurosci.* 8(10): 3658-3669.

McQuiston, A. R., and Katz, L. C. (2001). Electrophysiology of interneurons in the glomerular layer of the rat olfactory bulb. *J. Neurophysiol.* 86(4): 1899-1907. doi: 10.1152/jn.2001.86.4.1899

Meredith, F.L., Benke, T.A., and Rennie, K.J. (2012). Hyperpolarization-activated current (I_h) in vestibular calyx terminals: Characterization and role in shaping postsynaptic events. *JARO.* 13: 745-758. doi: 10.1007/s10162-012-0342-3.

Michel, C.B., Azevedo, C.C., Desmadryl, G., Puel, J.L., Bourien, J., and Graham, B.P. (2015). Identification and modelling of fast and slow Ih current components in vestibular ganglion neurons. *Eur. J. Neurosci.* 42(10): 2867-2877. doi: 10.1111/ejn.13021.

Mundiñano, I.C., Caballero, M.C., Ordóñez, C., Hernandez, M., DiCaudo, C., Marcilla, I., et al. (2011). Increased dopaminergic cells and protein aggregates in the olfactory bulb of patients with neurodegenerative disorders. *Acta. Neuropathologica.* 122: 61-74. doi: 10.1007/s00401-011-0830-2.

Nagayama, S., Homma, R., and Imamura, F. (2014). Neuronal organization of olfactory bulb circuits. *Front. Neural. Circuits.* 8: 98. doi: 10.3389/fncir.2014.00098.

Nai, Q., Dong, H. W., Linster, C., and Ennis, M. (2011). Activation of α1 and α2 noradrenergic receptors exert opposing effects on excitability of main olfactory bulb granule cells. *Neuroscience.* 169(2): 882-892. doi: 10.1016/j.neuroscience.2010.05.010.

Nickell, W.T., Behbehani, M.M., and Shipley, M.T. (1994). Evidence for GABAB-mediated inhibition of transmission from the olfactory nerve to mitral cells in the rat olfactory bulb. *Brain. Res. Bull.* 35(2): 119-123.

Panzanelli, P., Fritschy, J.M., Yanagawa, Y., Obata, K., and Sassoe-Pognetto, M. (2007). GABAergic phenotype of periglomerular cells in the rodent olfactory bulb. *J. Comp. Neurol.* 502(6): 990-1002. doi: 10.1002/cne.21356.

Parrish-Aungst, S., Shipley, M.T., Erdelyi, F., Szabo, G., and Puche, A.C. (2007). Quantitative analysis of neuronal diversity in the mouse olfactory bulb. *J. Comp. Neurol.* 501(6): 825-836. doi: 10.1002/cne.21205.

Pignatelli, A., Ackman, J.B., Vigetti, D., Beltrami, A.P., Zucchini, S., and Belluzzi, O. (2009). A potential reservoir of immature dopaminergic replacement neurons in the adult mammalian olfactory bulb. *Eur. J. Physiol.* 457: 899-915. doi: 10.1007/s00424-008-0535-0.

Pignatelli, A., and Belluzzi, O. (2017). Dopaminergic neurons in the main olfactory bulb: An overview from an electrophysiological perspective. *Front. Neuroanat.* 11:7. doi: 10.3389/fnana.2017.00007.

Pignatelli, A., Borin, M., Iseppe, A.F., Gambardella, C., and Belluzzi, O. (2013). The h-current in periglomerular dopaminergic neurons of the mouse olfactory bulb. *PLoS. One*. 8(2): e56571. doi: 10.1371/journal.pone.0056571.

Pignatelli, A., Kobayashi, K., Okano, H., and Belluzzi, O. (2005). Functional properties of dopaminergic neurones in the mouse olfactory bulb. *J. Physiol*. 564(2): 501-514. doi: 10.1113/jphysiol.2005.084632.

Pinching, A.J., and Powell, T.P. (1971). The neuron types of the glomerular layer of the olfactory bulb. *J. Cell. Sci.* 9: 305-345.

Ponsen, M.M., Stoffers, D., Booij, J., van Eck-Smit, Wolters, B.L.F., and Berendse, H.W. (2004). Idiopathic hyposmia as a preclinical sign of Parkinson's disease. *Ann. Neurol.* 56: 173-181. doi: 10.1002/ana.20160.

Puopolo, M., Bean, B.P., and Raviola, E. (2005). Spontaneous activity of isolated dopaminergic periglomerular cells of the main olfactory bulb. *J. Neurophysiol*. 94: 3618-3627. doi: 10.1152/jn.00225.2005.

Puopolo, M., and Belluzzi, O. (1998). Functional heterogeneity of periglomerular cells in the rat olfactory bulb. *Eur. J. Neurosci.* 10(3): 1073-1083. doi: 10.1046/j.1460-9568.1998.00115.x.

Ross, G.W., Petrovich, H., Abbott, R.D., Tanner, C.M., Popper, J., Masaki, K., et al. (2008). Association of olfactory dysfunction with risk for future Parkinson's disease. *Ann. Neurol.* 63(2): 167-173. doi: 10.1002/ana.21291.

Ross, M.T., Flores, D., Bertram, R., Johnson, F., and Hyson, R.L. (2017). Neuronal intrinsic physiology changes during development of a learned behavior. *eNeuro*. 4(5): e0297-17.2017 1-16. doi: 10.1523/ENEURO.0297-17.2017.

Sengupta, B., Faisal, A.A., Laughlin, S.B., and Niven, J.E. (2013). The effect of cell size and channel density on neuronal information encoding and energy efficiency. *J. Cereb. Blood. Flow. Metab.* 33(9): 1465-1473. doi: 10.1038/jcbfm.2013.103.

Shepherd, G.M. (1972). Synaptic organization of the mammalian olfactory bulb. *Physiol. Rev.* 52: 864-917. doi: 10.1152/physrev.1972.52.4.864.

Shepherd, G.M., Greer, C.A., Mazzarello, P., and Sassoe-Pognetto, M. (2011). The first images of nerve cells: Golgi on the olfactory bulb 1875. *Brain. Res. Rev.* 66(1-2): 92-105. doi: 10.1016/j.brainresrev.2010.09.009.

Suaud-Chagny, M.F. (2004). In vivo monitoring of dopamine overflow in the central nervous system by amperometric techniques combined with carbon fibre electrodes. *Methods.* 33(4): 322-329. doi: 10.1016/j.ymeth.2004.01.009.

Suaud-Chagny, M.F., Chergui, K., Chouvet, G., and Gonon, F. (1992). Relationship between dopamine release in the rat nucleus accumbens and the discharge activity of dopaminergic neurons during local in vivo application of amino acids in the ventral tegmental area. *Neuroscience.* 49(1): 63-72. doi: 10.1016/0306-4522(92)90076-e.

Tillerson, J.L., Caudle, W.M., Parent, J.M., Gong, C., Schallert, T., and Miller, G.W. (2006). Olfactory discrimination deficits in mice lacking the dopamine transporter or the D2 dopamine receptor. *Beh. Brain. Res.* 172(1): 97-105. doi: 10.1016/j.bbr.2006.04.025.

Trimmer, J.S., and Rhodes, K.J. (2004). Localization of voltage-gated ion channels in mammalian brain. *Annu. Rev. Physiol.* 66: 477-519. doi: 10.1146/annurev.physiol.66.032102.113328.

Vaaga, C.E., Yorhason, J.T., Williams, J.T., and Westbrook, G.L. (2017). Presynaptic gain control by endogenous cotransmission of dopamine and GABA in the olfactory bulb. *J. Neurophysiol*. 117: 1163-1170. doi: 10.1152/jn.00694.2016.

Wahl-Schott, C., and Biel, M. (2009). HCN channels: structure, cellular regulation and physiological function. *Cell. Mol. Life. Sci.* 66(3): 470-494. doi: 10.1007/s00018-008-8525-0.

Wei, C.J., Linster, C., and Cleland, T.A. (2006). Dopamine D(2) receptor activation modulates perceived odor intensity. *Behav. Neurosci.* 120(2): 393-400. doi: 10.1037/0735-7044.120.2.393.

Wilson, D.A., and Sullivan, R.M. (1995). The D2 antagonist spiperone mimics the effects of olfactory deprivation on mitral/tufted cell odor response patterns. *J. Neurosci*. 15(8): 5574-5581.

Zengel, J.E., Reid, S.A., Sypert, G.W., and Munson, J.B. (1985). Membrane electrical properties and prediction of motor-unit type of medial gastrocnemius motoneurons in the cat. *J. Neurophysiol.* 53(5): 1323-1344. doi: 10.1152/jn.1985.53.5.1323.

Zhang, H., and Sulzer, D. (2004). Frequency-dependent modulation of dopamine release by nicotine. *Nat. Neurosci*. 7(6): 581-582. doi: 10.1038/nn1243.

Zhang, L., Doyon, W.M., Clark, J.J., Phillips, P.E., Dani, J.A. (2009). Controls of tonic and phasic dopamine transmission in the dorsal and ventral striatum. *Mol. Pharmacol.* 76(2): 396-404. doi: 10.1124/mol.109.056317.

Figure captions

Figure 1

Rat OB and its endogenous DA neurons. **(A).** A horizontal OB slice with green fluorescent TH-GFP neurons localized to the GL. Discreet layers – ONL, GL, EPL, MCL, and GCL – deep to the GL were also emphasized with propidium iodide (red). Scale bar represents 200 μm. **(B).** A higher magnification of another OB slice with fluorescent DA neurons localized mostly to the GL, but also some neurons in the EPL, MCL, and GCL. Scale bar represents 100 μm. **(C).** A single spherical glomerulus with fluorescent DA neurons around its circumference. Scale bar represents 50 μm.

Dimensions of figure: 1476 pixels by 3300 pixels.

Figure 2

Comparison of membrane properties between OB DA neurons based on their localization in the GL and neuronal area. **(A)**. Top, red neurons = closer to ONL; Bottom, blue neurons = closer to the EPL. **(B).** Large, green neurons = 3390 to 4890 μm^2; Small, pink neurons = 1589 to 2610 μm^2). All data represented as mean ± SEM. **(C).** For membrane resistances (in MΩ), there was no significant difference (n = 64, p = 0.4181, **Ci**) between neurons based on their glomerular localization, but there was a significant difference (n = 48, p = 0.0001**, **Cii**) based on neuronal area. **(D).** For membrane capacitance (in pF), there was no significant difference (n = 64, p = 0.2979, **Di**) between neurons based on their glomerular localization, but there was a significant difference (n = 48, p < 0.0001****, **Dii**) based on neuronal area. **(E).** For neuronal areas (in μm^2), like capacitance, there was no significant difference (n = 64, p = 0.2979, **Ei**) based on glomerular localization. **(F).** For time constants (in ms), there was no significant difference (n = 64, p = 0.4153, **Fi**) between neurons based on their glomerular localization, and no significant difference (n = 48, p = 0.8786, **Fii**) between neurons based on neuronal area. **(G).** For action potential thresholds (in pA), there was no significant difference (n = 20, p = 0.1792, **Gi**) between neurons based on their glomerular localization, but there was a significant difference (n = 14, p < 0.0001****, **Gii**) between neurons based on area. **(H).** Frequency distribution of neuronal areas of DA neurons (2996 ± 94.72 μm^2, n = 73). Pink and green dashed borders are used to distinguish Small and Large neurons, respectively.

Dimensions: 180 mm (2 columns) by 82.1 mm.

Figure 3.

Action potential spiking properties of OB DA neurons. (**A).** There was no recorded spontaneous action potential activity (generated without stimulus input) in rat OB DA neurons. This recording shows synaptic activity, represented by EPSPs. (**B).** DA neurons fire a single action potential when stimulated with a sufficiently large depolarizing current. After firing an action potential, they go into depolarization block for the duration of the stimulus. These recordings resulted from incremental 10 pA steps, ranging from -10 to 80-pA. **(C).** A single trace from Figure 3B, which shows a single action potential generated from an 80-pA stimulus. (**D).** An example of a trace from a mitral cell (red trace), showing tonic firing in response to a 200-pA stimulus. (**E).** Some OB DA neurons fire multiple spikes when stimulated with a weaker stimulus (blue trace), but tend to fire a single spike with increasing stimulus strength (red trace). Each voltage trace is a response to incremental 25 pA stimuli, from -25 to 200 pA. (**F).** Example traces from Figure 3E, which show that a weak stimulus (25 pA in this example, blue trace) produced tonic action potential spiking, while a stronger stimulus (150 pA in this example, red trace) produced decaying spikes followed by a depolarization block. (**G).** To gauge if DA neurons have different spiking activity based on their glomerular localization and/or neuronal area, dummy variables were assigned to each spiking neuron (0 = no more than one spike at any depolarizing stimulus; 1 = multiple spiker at lower depolarizing stimuli only). There was no significant difference in average number of spikes between neurons based on their glomerular localization (n = 36, p = 0.7472, **Gi**), but there was a significant difference (n = 27, p = 0.0083**, **Gii**) between neurons based on neuronal area. Data represented as mean ± SEM

Dimensions: 180 mm (2 columns) by 163.75 mm.

Figure 4.

The voltage-gated I_{Na} in OB DA neurons. All recordings were performed in the presence of Cs and Cd. (**A).** Example of a group of I_{Na} from a DA neuron. These currents were activated by progressively depolarizing 200-ms 10 mV voltage steps, from -10 to 80 mV. Capacitance artifacts were manually blanked. **(B).** The current-voltage relationship (derived from 11 neurons)

showing peaks of I_{Na}. The largest peak amplitudes were produced when the membrane was depolarized between -20 and 0 mV. (**C**)**.** An example of the protocol used to derive the inactivation/h∞ curve in E. 50 ms pre-pulse voltage steps ranged from -90 to -30 mV in 10 mV steps. Test 100 ms test pulse was 80 mV. Each color of the protocol trace is coordinated with the color of the current trace. **(D).** An example of the protocol used to derive the removal of inactivation/interpulse interval curve in H. Neurons received paired voltage steps, depolarizing the membrane to 60 mV, with increasing subsequent interpulse intervals (.5, 1, 3, 5, 7.5, 10, 12.5, 15, and 50 ms). **(E).** The I_{Na} h∞ inactivation curve (derived from 23 neurons). Half of I_{Na} is inactive when the membrane is depolarized to -49 mV. **(F).** To gauge if I_{Na} inactivation properties differ between DA neurons based on their glomerular localization and/or neuronal area, their membrane voltages at 50% inactivation were compared. There was no significant difference between neurons based on localization (n = 23, p = 0.2149, **Fi**) or area (n = 13, p = 0.4645, **Fii**). **(G).** Inactivation curves were also compared between Top and Bottom (**Gi**) and Large and Small (**Gii**) neurons. For the membrane potentials of -70 and -60 mV, there were no significant differences between Top and Bottom neurons (-70 mV: n = 23, p = 0.1500; -60 mV: n = 23, p = 0.067), while there were significant differences between Large and Small neurons (-70 mV: n = 13, p = 0.0032**; -60 mV: n = 13, p = 0.0258*). **(H)**. The I_{Na} IPI curve (derived from 25 neurons). Currents were activated with two 60-mV, 20-ms depolarizing steps. The activation time constant (τ = 63% of the channels are activated) is 13 ms. (**I).** To gauge if I_{Na} reactivation properties differ between DA neurons based on their glomerular localization and/or neuronal area, the average τ were compared. There was no significant difference between neurons based on localization (n = 25, p = 0.9710, **Ii**) or area (n = 12, p = 0.2913, **Iii**). **(J)**. Individual IPI curves were also constructed for Top and Bottom (**Ji**) and Large and Small (**Jii**) DA neurons. These two sets of curves were similar. Data points are represented as mean ± SEM.

Dimensions: 180 mm (2 columns) by 270 mm.

Figure 5.

The hyperpolarization-activated, non-specific cation I_H in OB DA neurons is identified by upward voltage sags during hyperpolarization, afterhyperpolarization depolarization, and (sometimes) an action potential following hyperpolarizing stimuli. (**A).** An example of a DA

neuron showcasing these three properties of I_H during three hyperpolarizing current (-25, -50, and -75 pA) injections. (**B).** Representative hyperpolarizing traces of each of the four groups of DA neurons from this study (red = Top, blue = Bottom, green = Large, pink = Small). All traces are scaled to the scale on the bottom left of the figure. **(C).** A comparison of voltage sag ratios of DA neurons based on their glomerular localization and neuronal area. There was no significant difference between DA neurons based on their glomerular localization, either when the neurons received a -25-pA stimulus ("at -25 pA," n = 34, p = 0.4500, **Ci**) or when receiving a combination of -25, -50, -75 pA, or all three hyperpolarzing currents ("at all currents," n = 26, p = 0.5904, **Cii**). There were significant differences between DA neurons based on the neuronal area, both when receiving only a -25-pA stimulus (n = 26, p = 0.0061**, **Ciii**) and when receiving the combination of hyperpolarizing currents (n = 18, p = 0.0067**, **Civ**). (**D).** Voltage sag ratios of DA neurons were compared at starting membrane potentials positive to -120 mV. There was no significant difference between neurons based on glomerular localization (n = 49 sags, p = 0.6784, **Di**), but Small DA neurons had a significantly greater voltage sag ratio than Large neurons (n = 30 sags, p < 0.0001****, **Dii**). **(E).** Voltage sag ratios of DA neurons were also compared at membrane potentials negative to -120 mV. Again, there was no significant difference between neurons based on glomerular localization (n = 90 sags, p = 0.2576, **Ei**), but Small DA neurons had a significantly greater voltage sag ratio than Large neurons (n = 63 sags, p = 0.0432*, **Eii**). All data represented as mean ± SEM.

Dimensions: 180 mm (2 columns) by 185 mm.

Figure 6.

Analysis of the effects of ramp slopes (in pA/ms) on the ON and OFF currents of OB DA neurons. **(A).** Example of a ramp protocol (bottom) and a resulting voltage trace (top). The traces and their corresponding ramps were used to determine the ON (black circles) and OFF (white circles) currents. This figure also shows an example of how spike frequencies are derived from traces of ramp protocols (data shown in **Fig. 7**). Of the 42 ramps used, some ramps had identical slopes (e.g., the slope of 2 pA/ms can include ramps of 200 pA for 50 ms, 400 pA for 100 ms, etc.). For different ramp protocols with the same slopes, the ON and OFF currents and the spike frequencies and number of action potentials in the next figure were averaged. **(B)** Averaged ON

and OFF current responses to ramp slopes (derived from 19 neurons). Increasing the slope increases the ON and OFF current of all neurons, but the largest effect is on the OFF current. This also indicates a decrease in duration of spiking with increasing ramp slopes. **(C).** A comparison of ON and OFF currents of DA neurons based on their glomerular localization. After transforming these power functions into log-log plots (see Materials and Methods), there was no significant difference between the increasing ON ($n = 19$, $p = 0.3405$) and OFF currents ($n = 19$, $p = 0.5368$) with increasing ramp slopes between Top and Bottom neurons. **(D).** Same comparison between DA neurons based on their neuronal areas. There were no significant differences in the increasing ON current ($n = 10$, $p = 0.7680$) with increasing ramp slopes, but there was a difference in the increasing OFF currents ($n = 10$, $p = 0.0402$*) between Large and Small neurons. All data represented as mean ± SEM.

Dimensions: 85 mm (1 columns) by 185.31 mm.

Figure 7.

Analysis of the effects of ramp slopes on the spike frequencies and the number of spikes of OB DA neurons. **(A).** The frequency responses (in Hz) of neurons ($n = 13$) that spiked more than once per ramp stimulus increase with increasing ramp slopes. **(B).** After transforming these power functions into log-log plots (see Materials and Methods), there was no difference ($n = 13$, $p = 0.3544$) in the increasing spike frequencies with increasing ramp slopes between Top and Bottom DA neurons. **(C).** The increasing spike frequencies with increasing ramp slopes was significantly higher ($n = 7$, $p < 0.0043$**) in Small than Large neurons. **(D).** Number of spikes produced with increasing ramp slopes of neurons ($n = 13$) drops dramatically, particularly between 0 and 2 pA/ms ramps **(E).** Top DA neurons produced a significantly greater decrease in spikes across increasing ramp slopes than did Bottom neurons ($n = 13$, $p = 0.0009$***). **(G).** There was an even greater decrease in spikes across increasing ramp slopes in Large compared to Small DA neurons ($n = 7$, $p < 0.0001$****).

Dimensions: 180 mm (2 columns) by 143.42 mm.

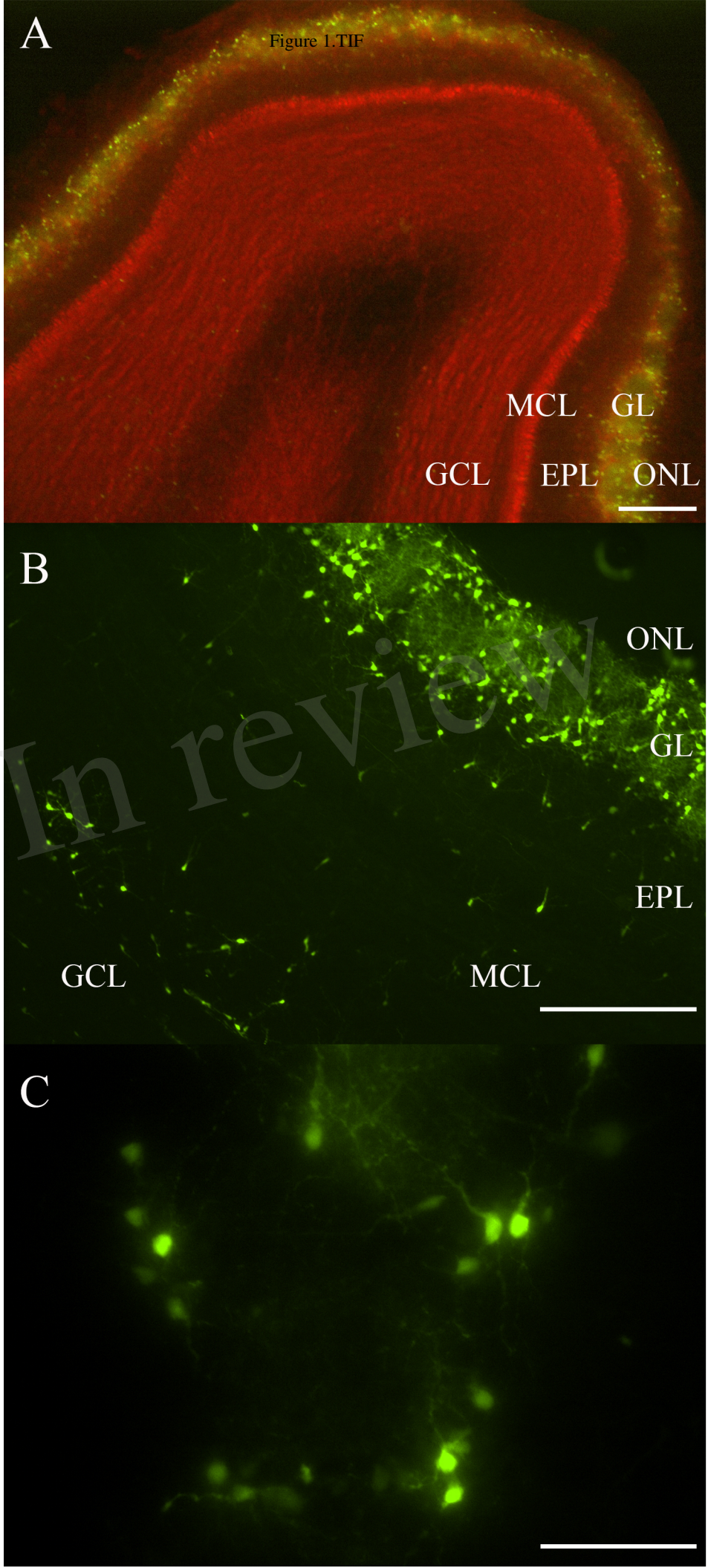

Figure 2.TIF

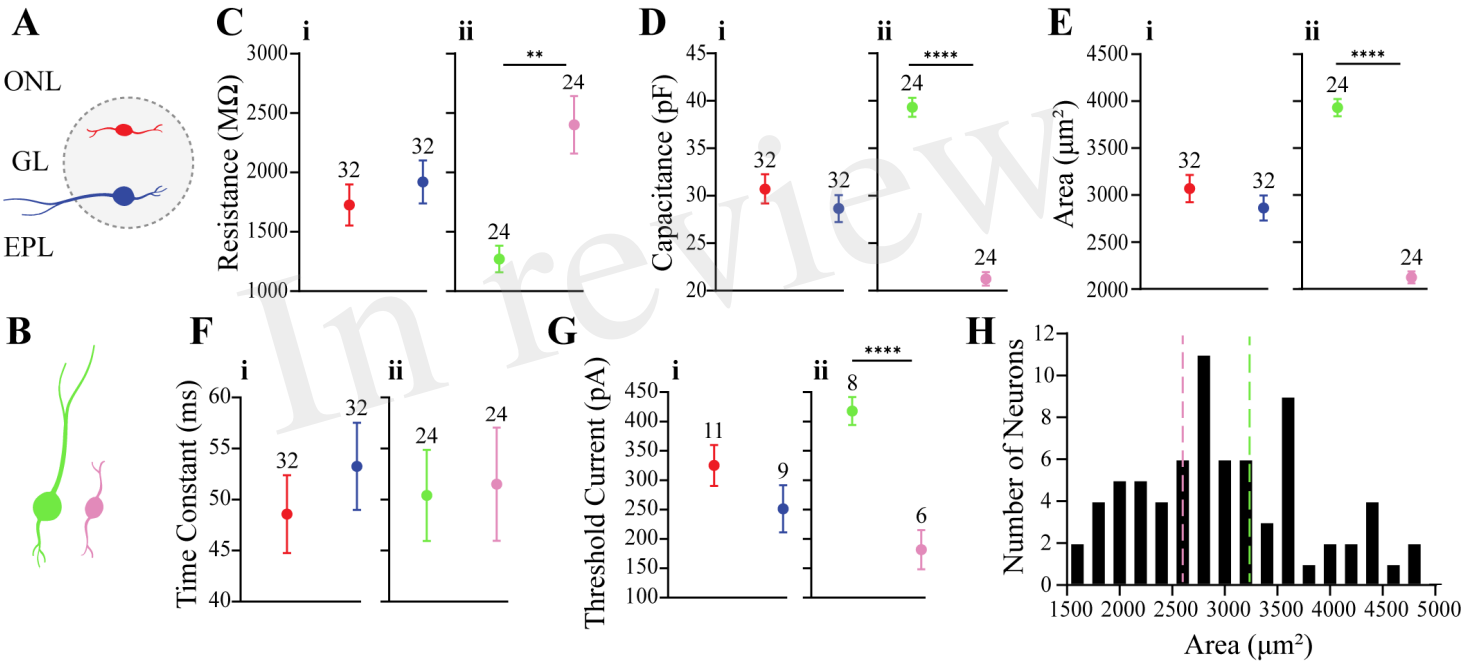

Figure 3.TIF

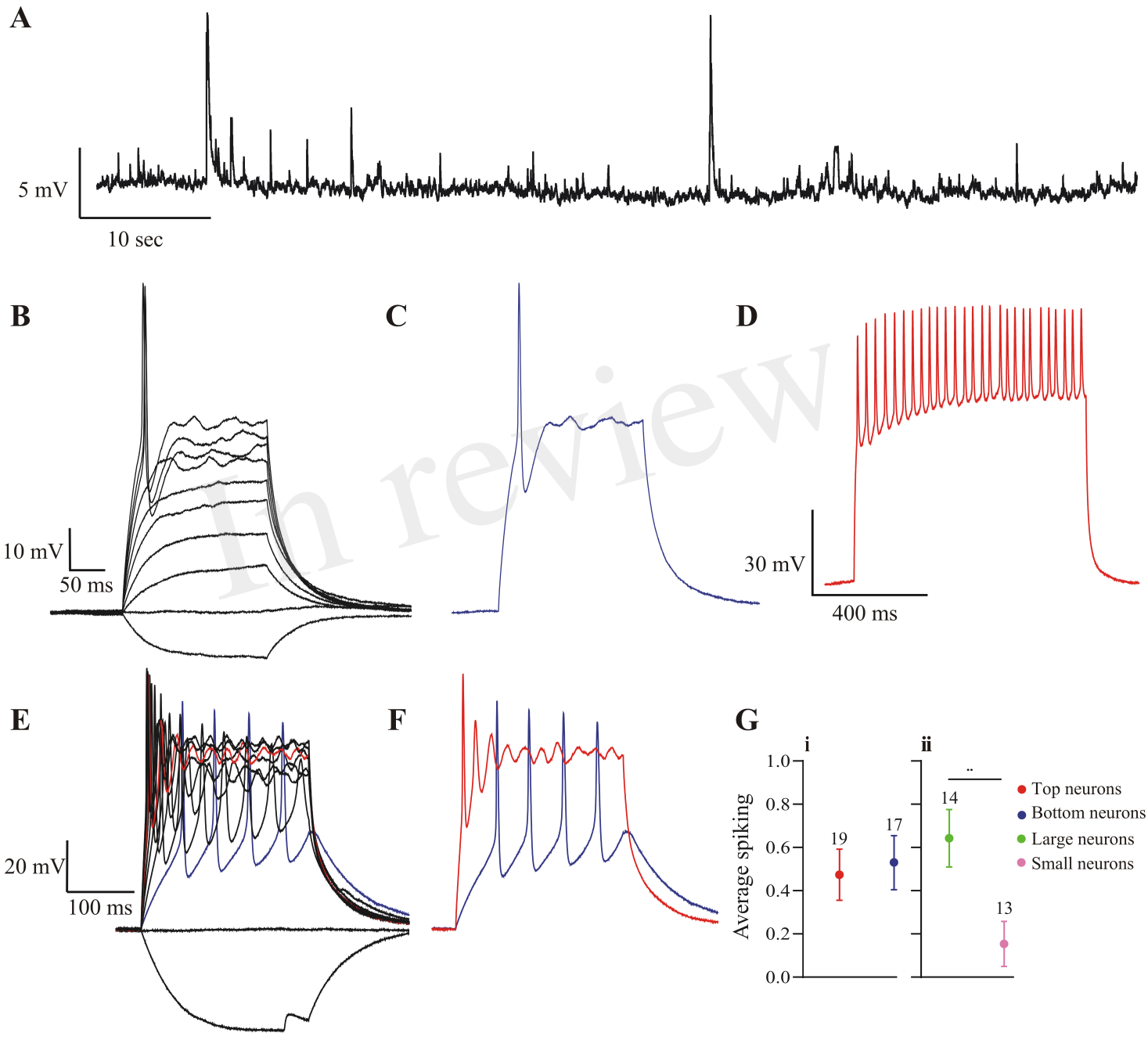

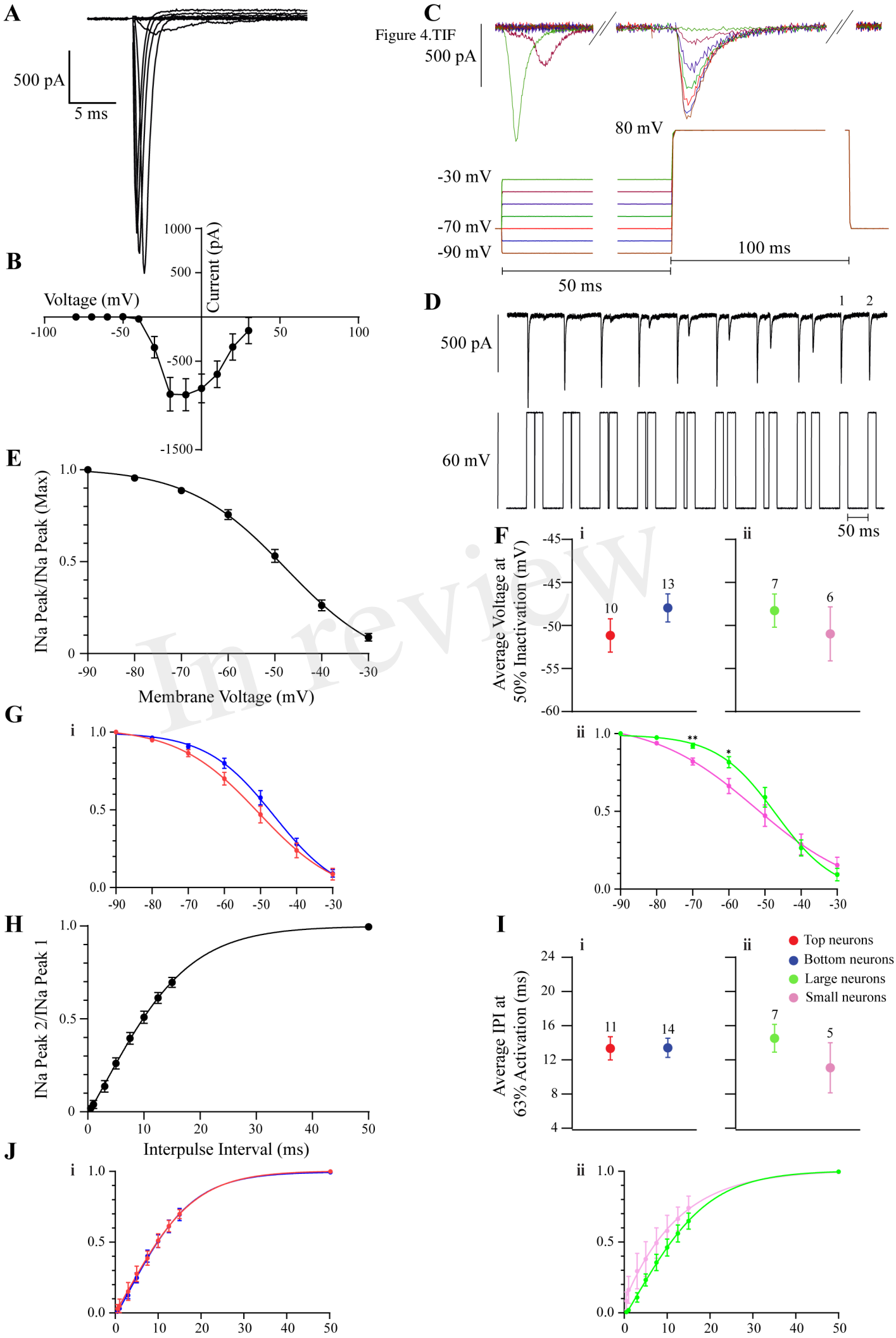
A
500 pA
5 ms
B
Voltage (mV)
Current (pA)
1000
500
-500
-1500
-100
-50
50
100
C
Figure 4.TIF
500 pA
80 mV
-30 mV
-70 mV
-90 mV
100 ms
50 ms
D
500 pA
60 mV
1
2
50 ms
E
INa Peak/INa Peak (Max)
Membrane Voltage (mV)
F
Average Voltage at 50% Inactivation (mV)
i
ii
10
13
7
6
G
i
ii
H
INa Peak 2/INa Peak 1
Interpulse Interval (ms)
I
Average IPI at 63% Activation (ms)
Top neurons
Bottom neurons
Large neurons
Small neurons
11
14
7
5
J
i
ii

Figure 5.TIF

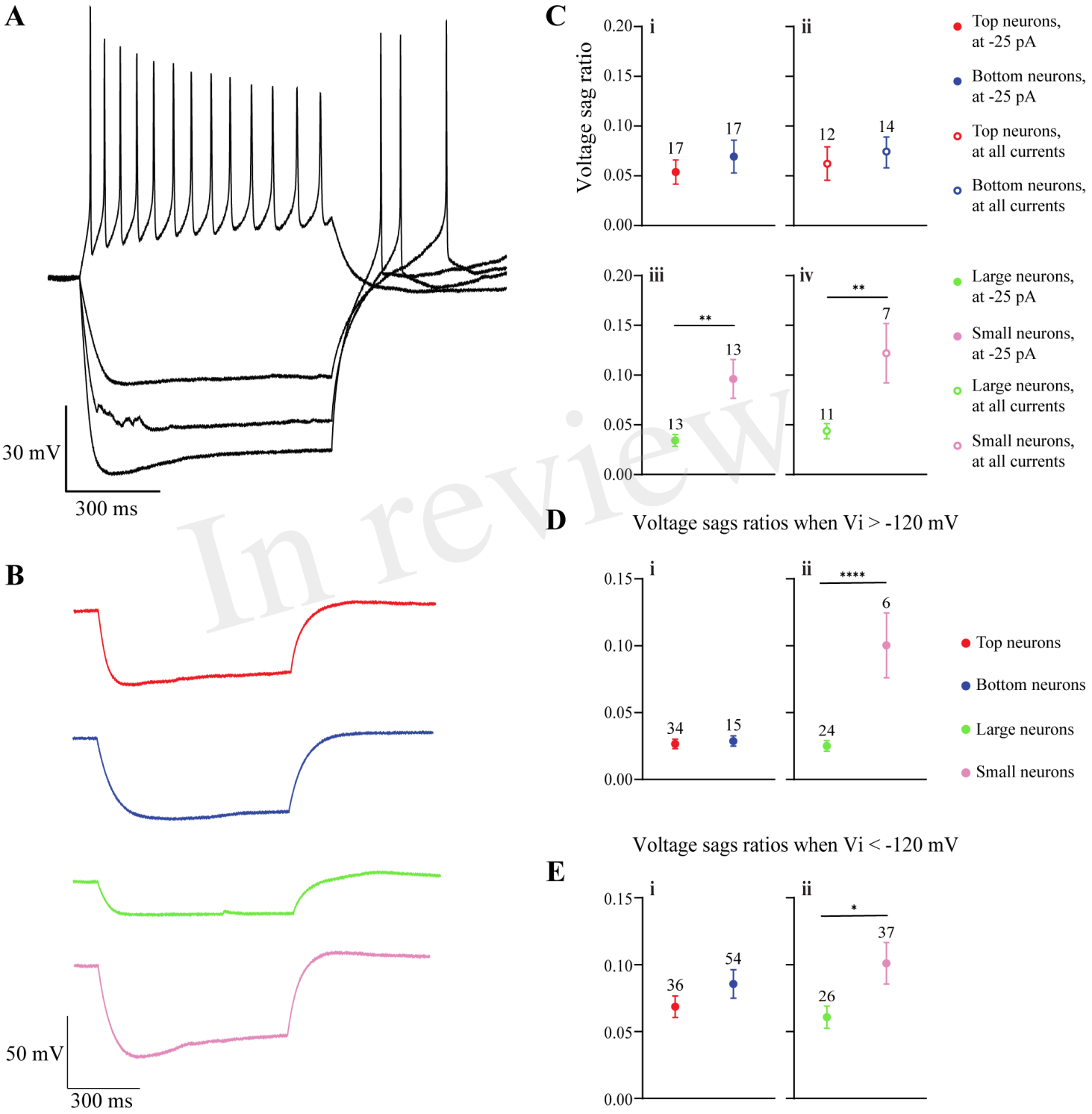

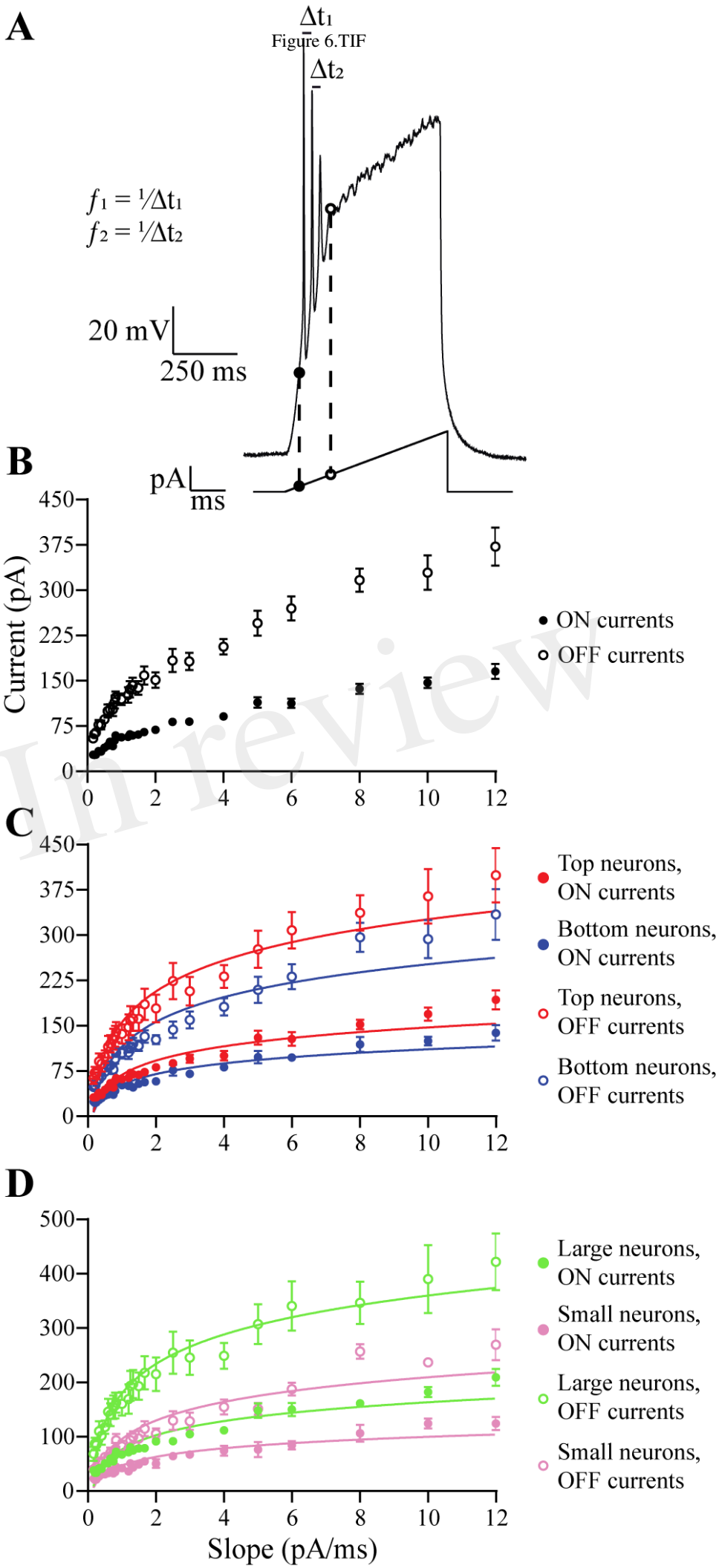

Figure 7.TIF